Summer 2011

Determining Lake Sedimentation Rates Using Radionuclide Tracers

Riley Aaren Post
University of Iowa

DETERMINING LAKE SEDIMENTATION RATES USING RADIONUCLIDE TRACERS

by

Riley Aaren Post

A thesis submitted in partial fulfillment
of the requirements for the Master of
Science degree in Civil and Environmental Engineering (Water Resources)
in the Graduate College of
The University of Iowa

July 2011

Thesis Supervisor: Professor Athanasios N. Papanicolaou

Graduate College
The University of Iowa
Iowa City, Iowa

CERTIFICATE OF APPROVAL

_____

MASTER'S THESIS

_____

This is to certify that the Master's thesis of

Riley Aaren Post

has been approved by the Examining Committee for the thesis requirement for the Master of Science degree in Civil and Environmental Engineering (Water Resources) at the July 2011 graduation.

Thesis Committee: _____
Athanasios N. Papanicolaou, Thesis Supervisor

_____
A. Jacob Odgaard

_____
Christopher G. Wilson

Knowledge speaks, but wisdom listens.
Jimi Hendrix

ACKNOWLEDGMENTS

I would like to thank Dr. Thanos Papanicolaou and Dr. Christopher Wilson for their unwavering support and guidance throughout the many stages of this project. Their patience and example have been essential in my development as a graduate student, researcher, and engineer over the past year. Thank you, also to Dr. A. Jacob Odgaard for graciously agreeing to sit on my defense committee, and for traveling back to Iowa City to do so. I would also like to thank my parents and brother; the former for their steady love, constant encouragement, and harsh motivation when it was especially needed; the latter for keeping me on my toes. Finally, I would like to thank my grandparents, all of whom have been incredibly influential to me at every phase of my life. Through each of their example I have learned the immeasurable value a good work ethic, humility, patience, integrity, and reverence to name very few. They never cease to inspire and support me, and for that I could not be more grateful.

ABSTRACT

The objective of this study was to determine the origin of sediment currently collected in Black Lake, an extremely productive salmon fishing environment located along a remote section of the Alaska Peninsula, AK. To meet the goals of this project, soil cores were collected at the site during an extensive field study. The field investigation was based on a prior numerical study, which revealed the most erodible areas and the hydrologic patterns in Black Lake and its tributaries, namely the Alec River. From this study, select locations of the catchment were chosen for coring. These included the Alec River Delta, Black Lake, and four tributaries in the catchment. These samples were analyzed for the radionuclides ^{137}Cs and ^{210}Pb to determine soil deposition rates using Gamma Spectroscopy. To determine the sedimentation rate of each coring location, spikes in the ^{137}Cs activity were connected to the known cesium deposition peak in 1964 and the depth of soil above the peak was divided by the number of years that have passed. This gave a spatially averaged deposition rate within the lake of roughly 0.25 cm/y. This result closely compared to the numerical study of Elhakeem and Papanicolaou (2008) and to a study done in close proximity to Black Lake in the early 1990s (Stihler et al. 1992). The rate of each location was then validated by visually analyzing each core using soil color demarcation lines to determine the soil composition. This analysis resulted in the discovery of a variety of soil types ranging from silts and clays, to coarse sands, to volcanic tephra. It was concluded that the lake flow patterns, the introduction of volcanic material from nearby Mt. Veniaminof, and back water resulting from deposition occurring down stream of Black Lake at the Black River's junction with the West Fork River are some of the main contributors for the deposition in the lake.

TABLE OF CONTENTS

LIST OF TABLES

LIST OF FIGURES

LIST OF NOMENCLATURE

A	Sample Activity
B	Background Activity
C	Sample Emission Rate
CIC	Constant – Initial – Concentration
CRS	Constant – Rate of – Sedimentation
D	Soil Grain Diameter
e_B	Background Activity Error
e_C	Emission Rate Error
e_E	Detector Efficiency Error
e_F	Self-Absorption Correction Factor Error
E	Detector Efficiency
F	Self-Absorption Correction Factor
F_m	Hydrometer Meniscus correction Factor
F_z	Hydrometer Zero Correction Factor
G	Acceleration of Gravity
G_s	Specific Gravity of Soil Grains
I	Unattenuated Photon Emission
K_d	Partition Coefficient
m	Mass of Sample (Spectroscopy Calculations)
M_s^0	Initial Mass of Soil (Hydrometer Test)
M_s	Dry Sample Mass (Bulk Density)
NF	North Fork
SF	South Fork
P	Porosity
P_f	Percent of Sample Finer than Specific Sieve
R	Branching Ratio

R_c	Hydrometer Correction Value
R_{mc}	Hydrometer Meniscus Correction Value
T	Attenuated Photon Emission
t	Time
$t_{1/2}$	Isotope Half Life
v	Particle Fall Velocity
V_t	Sample Volume (Bulk Density)
W_l	Liquid Weight
W_s	Solid weight
λ	Decay Rate
μ	Viscosity of Water
ρ_{BD}	Bulk Density
ρ_f	Density of Sodium Hexametaphosphate
ρ_l	Liquid Density
ρ_s	Particle Density

CHAPTER 1: INTRODUCTION

1.1 Sedimentation in Lakes

The process of erosion encompasses the following four stages: detachment, transport, redistribution, and deposition (Lal, 2005). Erosion begins in upland areas (i.e., hills and floodplain) when raindrops break soil aggregates into smaller soil particles as they impact the land surface. These detached soil particles are entrained by runoff from the accumulated rainfall as it travels downhill. The runoff transports and redistributes the eroded soil particles on the landscape. Depending on the runoff characteristics (e.g., depth and velocity), landscape gradient, and vegetative cover, a certain percentage of these particles stay in suspension and reach the stream channel (Julien et al., 1985; Huang et al. 1999).

In some parts of a watershed (i.e., uplands and stream reaches) for example water moves faster, carrying sediment downstream. The particles will continue to move downstream until the flow's transport capacity decreases until it is no longer sufficient to support a particle's weight (Huang et al., 1999). The transit times and travel distances of the entrained sediment are unique to a specific site or storm event, which complicates monitoring and analysis of watershed sediment dynamics.

The majority of this transported sediment will deposit once the material reaches the final sink area in the watershed, such as a lake. This is due largely to the stagnant nature of water within a lake when it is compared to the water moving as overland flow or in rivers and streams (Horne, 1994).

Flow velocities within lakes can be nearly negligible relative to the flow in the riverine parts of the watershed. Therefore, transport capacities are low and the water

cannot support sediment transport. Under these conditions, the sediment begins to settle out and deposits on the lake bed, as well as creating deltas, sand bars, and sand spits (Kendall, 1998).

The rates of sediment accumulation on the lake bed will vary throughout the lake depending on (1) the relative deliveries of sediment from the surrounding tributaries and watershed and (2) the circulation patterns within the system due to wind and lake currents. Over time, heterogeneous deposition patterns will develop in a lake and can alter its flow patterns drastically. In addition, sediment deposition can lead to infilling of the lake completely, especially if the delivery rates have been enhanced by anthropogenic or climatic activity (e.g., Meade et al., 1990; Hooke, 1994; Stallard, 1998). Changes in lake storage resulting from the infilling will also affect the habitat of aquatic species through changes in resource allocation and living conditions such as water temperature (e.g., Ruggerone et al., 1999). Finally, nutrients and other contaminants associated with the incoming sediment can further degrade the system through increasing toxicity levels and hypoxia (e.g., Edmondson et al., 1956; Rabalais et al., 2010).

It is for these reasons that it is of critical importance to effectively monitor lake sedimentation in trying to better understand the involved processes. Better understanding can lead to better, more specific, plans for lake restoration. Thus, the focus of this study was to evaluate specific sedimentation rates within a threatened watershed on the Alaskan Peninsula using radionuclide tracers. This study will provide the first time direct measurements of deposition in this remote setting.

1.2 Determining Sedimentation using Radionuclide Tracers

A variety of methods exist in determining sedimentation rates in lakes, one such method being the use of radionuclide analysis through gamma spectroscopy. Gamma spectroscopy provides a simple and non-destructive means of determining infilling rates through either the identification of temporal markers in the stratigraphy of a lake bed or quantifying the radionuclide activities at specific soil depths (Begy et al., 2009 and Kanai, 2011). A sedimentation rate can be determined by developing graphs of the radionuclide activity vs. depth in the sediment column (Fauer, 1986). From these graphs, the sedimentation rates is calculated by dividing the depth of soil by the radionuclide temporal marker with the amount of time that has passed since the deposition of that marker (Ritchie and McHenry, 1990) or by fitting a line through the activities, depending on the specific radionuclide analyzed. The two such radionuclides that are most often used for this analysis are Lead-210, ^{210}Pb, and Cesium-137, ^{137}Cs (e.g. Sanders, 2010 and Wallbrink, 1993).

Lead-210 (half-life, $t_{1/2}$ = 22 years) is a daughter product of Uranium-238, ^{238}U ($t_{1/2}$ = 4.5 x 10^9 years) series. Uranium-238, which resides predominantly in landscape soils, decays through a series of daughter products to gaseous Radon-222, ^{222}Rn ($t_{1/2}$ = 4.5 x 10^9 years). A portion of the ^{222}Rn diffuses into the atmosphere, while some remains in the soil. Radon-222 further decays through a series of short-lived daughters to ^{210}Pb. The ^{210}Pb in the atmosphere attaches to aerosols which eventually deposit on the earth's surface through precipitation events (i.e., rain and snow) (Mabit, 2008). The ^{210}Pb produced within the soil is termed "supported", while the atmospheric ^{210}Pb is termed "excess" (i.e., $^{210}Pb_{xs}$) and is used in sedimentation studies. Upon delivery to the

landscape, the ^{210}Pb quickly and strongly bond to surface silt and clay particles (He et al., 1996) through cation exchange. When these finer soil particles are eroded and transported to the downstream lakes, the radionuclide remains attached. Upon entering the lake system, the ^{210}Pb and sediment will deposit on lake bed (Mizugaki, 2006). However, the distribution of ^{210}Pb within a soil column can be intermittent, based on wind fluxes and variations in the amount of ^{222}Rn released by the earth over a given time period. As a result, the evaluation of ^{210}Pb in the soil column is best suited for areas where the ^{210}Pb flux and sedimentation rates have stayed constant over time (Kendall, 1998).

In contrast to ^{210}Pb, the other radionuclide, ^{137}Cs, was derived from an anthropogenic source, namely the fallout from atmospheric nuclear tests completed in the 1950s and 1960s, and occasional releases during nuclear accidents (e.g., Chernobyl in 1986). Essentially, prior to 1952, all the ^{137}Cs on earth had decayed away. However, the atmospheric testing of atomic bombs conducted from 1952 to 1964 (prior to the Partial Nuclear Test Ban Treaty) by the United States and U.S.S.R re-released ^{137}Cs into the atmosphere.

Once in the atmosphere, ^{137}Cs attaches to aerosols and eventually deposits on the landscape, similar to ^{210}Pb. Upon delivery to the ground, the ^{137}Cs also quickly and strongly bonded to surface silt and clay particles (He et al., 1996 and Hughes et al., 2009) through cation exchange. The ^{137}Cs remains attached to these soil particles as they are detached, transported, and deposited in downstream lakes.

Activities of ^{137}Cs can be related to major, historical nuclear events correlating to the atmospheric nuclear tests (Li et al., 2011). These include the re-release in 1952, the peak testing period in 1964, the Chernobyl disaster that occurred in the former Soviet

Union in April of 1986, and possibly the nuclear disaster in Japan resulting from the large Tohoku earthquake and resulting tsunami in 2011. In studies within the North American continent, the spike related to 1986 Chernobyl disaster were small or unnoticed, which eliminates using this peak as a temporal marker in this study (Golosov, 1999).

In fluvial regions with high sediment loads, the different peak activities of ^{137}Cs can be found at varying depths within the soil column resulting in different sedimentation rates within a watershed. Higher sediment deposition rates will result in the peak activities being deeper in the soil column than in environments that are more stable (Kendall, 1998). However, in most lake environments, sedimentation rates will vary across the lake bed due to differences in the flow regimes relating to tributaries (with those varying between small and large contributors), surface runoff, and lake circulation patterns. This is well illustrated in the Alec River and Black Lake system on the Alaska Peninsula, Alaska.

1.3 Alec River and Black Lake System, AK: Problem Statement

Black Lake is a freshwater lake situated along a remote, mountainous section of the Alaskan Peninsula. The Black Lake system supports one of the world's largest populations of sockeye salmon (*Oncorhynchus nerka*), which is a central component of the local and statewide economy.

At full capacity, the water surface area of the lake is approximately 43 km^2, with a depth of 1.9 m. The primary tributary to Black Lake is the Alec River (known as the Squaw River by area natives), but it also receives nominal flows over land and through a

series of four tributaries from the west and north. The lake drains to the Black River, which flows south into Chignik Lake and finally, the Pacific Ocean (Elhakeem et al., 2008). At the outlet, the water depth is less than 0.5 m, but the bed elevation drops nearly 3 m before entering the Black River. Due to its size, relatively shallow depth, and the drop at the outlet, the lake has unique circulation patterns that were simulated by Elhakeem and Papanicolaou (2009) and were visually confirmed by a field study in 2010.

Many of the local fishermen and visiting University of Washington fishery scientists have noted a substantial change in the water storage volume of Black Lake since the late 1960s (Ruggerone et al., 1999). The change in lake volume has resulted in premature migration of the young salmon from Black Lake to Chignik Lake (Ruggerone, 1994), which detrimentally affects the adult returns to Chignik Lake. One possible explanation is the low water volume produces adverse conditions, namely warmer water temperatures that promote early migration downstream (Ruggerone et al., 1999). Increased sedimentation would result in faster infilling of the lake, thereby further reducing the water storage volume and exacerbating the problem of early salmon migration downstream.

The overarching issue that this project aims to tackle is a large amount of sediment building up within Black Lake. The ever-increasing amount of sediment within Black Lake is beginning to adversely affect the salmon population within the catchment by increasing temperature and creating low oxygen habitat conditions (Griffiths, 2011). This has serious implications for the villagers that inhabit the area, as it is their main source of food revenue.

The main objective of this study is to determine the sedimentation rates occurring within the Black Lake water body using radionuclide tracers ^{137}Cs and ^{210}Pb. Through this method it may be possible to identify areas of large accumulation, the sediment provenance, and to begin outlining possible measures to reduce the amount of incoming sediment. Data from this study may support future numerical modeling of the Black Lake system.

1.4 Thesis Outline

This thesis contains the following five chapters: Introduction, Objectives, Methods, Results, and Conclusions. The Introduction chapter explains the background information of this study on Black Lake, and establishes the concerns and objectives this thesis aims to tackle. In Chapter 2: Objectives the goals of this study are outlined in detail, including the sub-objectives deemed essential to project completion. The Methods Chapter outlines the procedures used for the visual, grain size, and radionuclide analyses, and how each phase relates to obtaining results. The Results Chapter presents the findings of the aforementioned procedures and their relevance, and correlation, to previous studies. The Conclusions summarizes the study as well as discusses its limitations and opportunities for future work regarding sedimentation in the Black Lake, AK system.

CHAPTER 2: OBJECTIVES

The main objectives of this project were (1) to develop a geotechnical description of the sediment in Black Lake, AK and (2) to quantify sedimentation rates in the lake using the radionuclides, ^{137}Cs and ^{210}Pb. Black Lake is a very productive salmon fishing area, and the salmon fishing industry is the main source of income for local villagers on the Alaskan Peninsula. A recent reduction in the lake's storage volume has dramatically affected the salmon stock, and threatened the livelihood of these local villagers (Ruggerone 1994, 2003). The potential causes for the decreasing lake volume can be either hydrological (e.g., changes in water influxes or effluxes) or geomorphological (e.g., increased sedimentation or local scour at the lake outlet). This study will focus on the role of increased sedimentation in Black Lake.

In order to determine the sedimentation rates in the Black Lake system, a field study was conducted where cores from strategic locations of the lakebed were collected. In addition to quantifying sedimentation rates, a sedimentological analysis of the lake bed sediments involving the determination of a particle size distribution will be conducted to identify the provenance of the sediment being deposited in Black Lake.

CHAPTER 3: METHODS

The central objectives of this study were (1) to develop a geotechnical description of the sediment in Black Lake, AK and (2) to quantify sedimentation rates in the lake using the radionuclides, ^{137}Cs and ^{210}Pb. This chapter provides a detailed description of the Black Lake system and the procedures used throughout the study to obtain the geotechnical analysis and sedimentation rates.

3.1 Study Site

This section provides a general overview of the Black Lake system, which is located on the Alaska Peninsula near Chignik Lake, AK. For this thesis, the Black Lake system is defined as Black Lake, the network of streams discharging into the lake, and the lake outlet that empties to the Black River.

Black Lake is a freshwater lake centrally located on the Alaska Peninsula. The Alaskan Peninsula is a narrow stretch of land, which extends west from the southern part of Alaska to the Aleutian Islands, see Figure 3.1. The width of the Alaskan Peninsula at the location of Black Lake is approximately 85 km. North of the peninsula is Bristol Bay, which is a highly productive salmon fishing ground, while south of the peninsula is the Pacific Ocean.

The peninsula is comprised of steep mountains, flat plains, and numerous rivers, which drain into small lakes. The gradient of the Black Lake watershed is approximately 1% in the surrounding plains and up to a 23% in the mountainous areas (Chignik Topo Maps A5 and B4, 2011).

Volcanoes are also present on the peninsula, including Mt. Veniaminof. Mt. Veniaminof is an active volcano, which has had more than 10 small eruptions since 1930, with the most recent being on February 22, 2008 (Veniaminof Description and Statistics, 2011). The 2500-m tall volcano is only 36.2 km from Black Lake to the southwest. However, its full influence on Black Lake is unknown.

The significance of Black Lake in this region lies in its connection to the salmon fishing industry of local villagers on the Alaskan Peninsula. A recent reduction in the lake's storage volume has dramatically affected the salmon stock and threatened the livelihood of these local villagers (Ruggerone 1994, 2003). Black Lake at its full water storage capacity has a surface area of approximately 43 km^2 and a shallow depth of 1.9 m (Elhakeem et al., 2008).

The lake is fed primarily by mountain streams with some contributions from overland flow, which results from flood flows forced out of stream channels due to beaver dams. The main tributary to the lake is the Alec River, which flows into Black Lake from the east. The Alec River meanders approximately 29 kilometers from its headwaters, where it is a gravel-bed, step-pool channel. The channel transitions to a sandy bed stream before it empties into Black Lake.

In addition, the Alec River forms a delta where it enters the lake. On this delta, the Alec River forks approximately 2 km upstream of Black Lake forming two separate channels flowing north and south. This delta is heavily vegetated, which illustrates its stability. It is believed that high sediment loads from the Alec River watershed, which led to the formation of a delta, blocked the main channel. Two potential sediment sources in

the Alec River watershed are mountain deposits and channel banks, which show heavy erosion as they are severely undercut at the water's surface.

Aside from the Alec River, four small tributaries line the western and northern shores of Black Lake. These tributaries are Cottonwood, Crooked, Canoe, and Linhome Creeks and vary in length (4.7, 9.4, 13.3, and 9.6 km, respectively), as well as width (19.0, 30.1, 62.3, and 16.3 m, respectively), see Figure 3.2. Little information is available about the influence that these tributaries have on the storage volume of Black Lake. However, beavers build dams across these tributaries that nearly cut off the flow and sediment supply to the lake. These dams exist until the next large flood removes them resulting in an immediate influx of the water and sediment from behind the dams.

The water surface elevation of Black Lake is not only controlled by the surrounding stream network, but also by southeast - northwest winds, which can cause fluctuations in flow depths greater than 0.33 m. In conjunction with lake circulation patterns, these winds have produced a sand spit that is forming off the southern half of the Alec River delta. This sand spit is a unique feature of Black Lake and is a general concern because the spit may eventually cut off the southern basin from the rest of the lake, which would severely decrease the storage volume.

Black Lake drains from the southern basin into the Black River. At the outlet, the water depth quickly shallows to less than 0.5 m forming a step. Immediately beyond this step, water depths drop by nearly 3 m. From the Black River, the water flows to Chignik Lake and eventually the Pacific Ocean (Elhakeem et al., 2008).

Black Lake is a system that is very conducive to salmon habitat and spawning, and supports a large salmon population. Thus, Black Lake is among the most productive

salmon fisheries in the world, and is why a drastic change of habitat within the catchment is of such great concern to locals.

3.2 Core Extraction

Sediment cores were collected from the lakebed in strategic locations to determine the sedimentological characteristics of the lake sediments and to evaluate the radionuclide profiles within the lake sediments for quantifying long-term sedimentation rates using excess ^{210}Pb and ^{137}Cs. These locations were determined based on the flow circulations patterns determined in Elhakeem and Papanicolaou (2009), which were confirmed with visual assessments at the site. The primary areas for coring in the Black Lake system were near the outlet of the lake and the delta region of the Alec River. In addition, cores were collected from the mouths of the four smaller tributaries.

Long cores (~1 m deep) were collected at each site using core tubes consisting of 2-in. (5.08-cm) diameter PVC pipe. The tubes were manually pushed into the bed up to 1 meter. The top of the tube was sealed to create a vacuum and prevent the sediment from slipping out of the core tube, as seen in Figure 3.3a. The bottom of the tube was also capped immediately upon reaching the sediment-water interface. The cores were extruded on-site and cut into 2.5cm sections. The cores were weighed immediately after sectioning and shipped back to IIHR – Hydroscience & Engineering for further analysis.

Upon returning to the lab, the cores were "reconstructed" by organizing them into their respective cores. The samples were then oven dried to a consistent weight at 60^{o} C for 48 hr by convention. The wet and dry weights were used to calculate porosity (P) using the following equation:

$$P = \left(\frac{W_l}{W_s}\right)\left(\frac{\rho_s}{\left(\rho_1 + \frac{W_l}{W_s}\rho_s\right)}\right) \qquad \text{Eq. 3.1}$$

where W_l = the liquid weight; W_s = the solid weight; ρ_s = the density of the solid; and ρ_l = the density of the liquid (Behrens, 1980). After drying, the samples were photographed for later visual evaluation and then lightly crushed to a size less than 2mm for further analyses (i.e., quantifying radionuclide activities and particle size distribution.

3.3 Particle Size Analysis

Two different particle size analyses (i.e., sieve and hydrometer analyses) were performed in this study to determine the texture of each core. The sieve analysis provided a particle size distribution for the coarse grain sediments (i.e., sand and gravel), while the hydrometer analysis provided a particle size distribution for the fine grain sediments (i.e., silt and sand).

The sieve analysis was begun by lightly crushing each oven-dried sample to a size less than 2mm and recording the sample mass. A series of sieves were used (sieve numbers 20, 40, 60, 100, 140, 200), which corresponded to a range of particle sizes (0.84, 0.42, 0.25, 0.15, 0.125, and 0.074 mm, respectively). along with a pan to collect the fine particles. The sieves were cleaned and pre-tared using a mass balance. The sieves were then assembled according to decreasing pore size with the largest pore size on top and the pan on the bottom. The sample was then added to the top sieve, and the sieve nest was placed on the shaking apparatus for approximately 10 minutes. The sieves were then removed from the shaking apparatus and carefully separated. Each sieve and the

associated sediment were weighed on the mass balance and the weights were recorded to determine the coarse grain particle size distribution.

The hydrometer method was used to determine the particle size distributions of the fine grained sediment particles in each sample. This procedure is based on the settling velocity of a sediment particle with a known diameter, which can be expressed using Stokes Law below:

$$v = \frac{\rho_s - \rho_f}{18\mu} g D^2 \qquad \text{Eq. 3.2}$$

where v is the particle fall velocity, ρ_s is the mass density of the soil particle, ρ_f is the mass density of the sodium hexametaphosphate and water solution, μ represents the viscosity of water, g is the gravitation constant, and D is the soil grain diameter.

A 50-g sub-sample of each core interval was measured and mixed with 125mL of the 4% sodium hexametaphosphate solution for 10 hours. The solution was then flushed into a 1000-mL glass cylinder, which was then filled to the 1000-mL mark with deionized water. The mixture was stirred for two minutes and the hydrometer was then inserted into the glass cylinder. This time was recorded as t=0. Hydrometer readings (R_{ACT}) were taken at 0.25, 0.5, 1, 2, 4, 8, 15, 30, 45, 60, 75, and 90 minutes after the initial mixing of the sample and deflocculating solution. Addition readings were taken at 24 and 48 hours. After an observed reading at t=4min. the hydrometer was removed and kept in the 1000mL graduated cylinder that contained water and defloculating agent. The hydrometer was only reinserted in the soil bath at the remaining time intervals in order to take readings. After each subsequent reading the hydrometer was removed and placed in the 1000mL graduate cylinder for cleaning.

The hydrometer test uses multiple constants, which must be determined to calibrate the results from the readings. The hydrometer was calibrated by taking a reading and subtracting the value from 1.000. This procedure will find the zero correction factor (F_z). The meniscus correction (F_m) (the distance from the top of the meniscus to the water's surface) was also observed. These values are determined using a control. The control consists of a separate 1000mL graduated cylinder, 875mL of distilled water and 125mL sample of the flocculating agent. The flocculating agent is a 4% sodium hexametaphosphate solution.

The fine particle size distribution was determined using Eq. 3.3 and Eq. 3.4 below, respectively, the meniscus correction value (R_{mc}) and hydrometer correction value (R_c) were determined and recorded.

$$R_{mc} = R_{ac} + F_m \qquad \text{Eq. 3.3}$$

$$R_c = R_{mc} - F_z + C_T \qquad \text{Eq. 3.4}$$

After all other values were recorded the percent finer value (P_f) could be found using Eq. 3.5.

$$P_f = \left(\frac{1000}{M_s^0}\right)\left(\frac{G_s}{(G_s - 1)}\right)(R_c - 1)100\% \qquad \text{Eq. 3.5}$$

where G_s is the specific gravity of the soil grains.

3.4 Radionuclide Analysis

Gamma Spectroscopy was used to determine the activities of ^{137}Cs and ^{210}Pb in the sediments samples of the cores. It is an established method used to measure the decay of radioactive material, which is simple and non-destructive. Preparation of samples for

Gamma Spectroscopy analysis is minimal and includes only drying, light crushing, and sealing the sample in a Petri dish. One drawback of this method is the substantial analysis time (~1 day), which is due to the low activities associated with environmental samples. Sediment particles are tagged with only the atmospheric delivery of ^{137}Cs and ^{210}Pb. The long analysis time constrains the number of collected samples.

Radioactive isotopes will emit photons at discrete and unique energy levels (i.e., gamma energy) during the decay process. The amount of emitted gamma energy at each discrete energy level is a statistically constant fraction of the total number of decays (or branching ratio). The activity at one of these discrete energies can be used to quantify the total activity of the isotope (Bonniwell, 2001). In this project, the radionuclides of interest were ^{137}Cs, ^{210}Pb, and ^{214}Bi. The activity of ^{210}Pb was determined at 46.5 keV and ^{137}Cs at 661 keV with ^{214}Bi at 609 keV.

Gamma Spectroscopy detectors (Figure 3.4) apply a high voltage across a High Purity Germanium (HPGe) crystal. The photon energy striking the crystal is converted into a voltage, which is translated by a computer as an activity (Bonniwell, 2001).

The efficiency of HPGe Gamma Spectroscopy detectors at measuring the photon emissions is a function of multiple variables (Bonniwell, 2001) including the size and shape of the germanium crystal, as well as the sample shape and size, which affect the portion of emissions striking the crystal. Thus, standards must be made that include radionuclides emitting a wide range of photon energies for calibration. Standards were constructed to calibrate the above detector for this study. The methods for standard preparation and detector calibration were similar to those in Wilson et al. (2003), Kuhnle et al. (2008), and Denn (2010). Two different Standard Reference Materials (SRMs),

which contain a suite of radionuclides including ^{137}Cs and ^{210}Pb, were used during calibration and analyzed in polystyrene Petri dishes (48 mm D x 8 mm H). Moreover, background activities must be accurately quantified and subtracted from the total activity measured for each sample.

A Gamma Spectroscopy lab has been established at IIHR – Hydroscience & Engineering in Iowa City, IA to facilitate the analysis of the samples for this study (Figure 3.4). The HPGe detector used in this lab contains a low background cryostat and a 4-in. lead shield with copper and titanium linings. The high purity germanium crystal with a carbon fiber window has a 69.7-mm diameter and a 27.6-mm length. The performance statistics before and after shipping either met or exceeded factory certification.

Individual samples were analyzed polystyrene Petri dishes (48 mm D x 8 mm H) on the HPGe gamma detector for at least 82800 seconds and then for an additional 300 seconds with a standardized sealed source to account for self-adsorption of the ^{210}Pb photon (Cutshall et al., 1983). The net emission rates were then corrected for sample geometry, detector efficiency, branching ratio, and radioactive decay (to the day of collection). The equation to determine activity, A, (Bq/g) is:

$$A = \frac{(C - B)e^{(-\lambda t)}}{m * E * R} \qquad \text{Eq. 3.6}$$

where C is the emission rate (counts/second), B is the background (ambient) activity, λ is the decay rate (d^{-1}), t is the difference between collection date and counting date (d), m is the mass of sample (g), E is the detector efficiency, and R is the branching ratio. This

equation applies to ^{137}Cs. The error of the activity (e_A) was calculated from the propagation of error described in Taylor (1997) and is:

$$e_A = A\sqrt{\frac{\left(\frac{e_c^2 + e_B^2}{R}\right)}{\left(\frac{C-B}{R}\right)^2 + \left(\frac{e_E}{E}\right)^2}} \qquad \text{Eq. 3.7}$$

where e_C is the error of the emission rate, e_B is the error of the background activity, and e_E is the error of the efficiency. All other variables are similar to those in Eq. 3.6. The ^{210}Pb activities were calculated using the following equation:

$$A = \frac{(C-B) * F * e^{(-\lambda t)}}{m * E * R} \qquad \text{Eq. 3.8}$$

where all variables are the same as in Eq. 3.6, except F is the self-absorption correction factor. The equation to determine the self-absorption correction factor (Cutshall et al., 1983) is:

$$F = \frac{\ln(T * I)}{\left[\left(\frac{T}{I}\right) - 1\right]} \qquad \text{Eq. 3.9}$$

where T is the attenuated photon emission and I is the unattenuated photon emission through a blank or empty sample. The error of the activity was determined based on the propagation of error described in Taylor (1997) and is:

$$e_A = A\sqrt{\frac{\left(\frac{e_c^2 + e_B^2}{R}\right)}{\left(\frac{C-B}{R}\right)^2 + \left(\frac{e_E}{E}\right)^2 + \left(\frac{e_F}{F}\right)^2}} \qquad \text{Eq. 3.10}$$

where e_F is the error of the correction factor from Eq. 3.9. All other variables are similar to those in Eq. 3.7.

Quality assurance was established using the NIST Ocean Sediment Environmental Radioactive Standard (SRM 4357). The SRM has a certified activity of ^{137}Cs of 0.013 ± 0.001 Bq/g and a range of 0.011 to 0.016 Bq/g. The SRM has uncertified activities of ^{210}Pb and ^{214}Bi. The range of activities for ^{210}Pb is 0.014 to 0.035 Bq/g; the range of activities for ^{214}Bi is 0.009 to 0.020 Bq/g. Measured activities averaged 0.010 ± 0.001, 0.024 ± 0.004, 0.012 ± 0.001 Bq/g (n = 3) for ^{137}Cs, ^{210}Pb, and ^{214}Bi, respectively.

3.5 Sedimentation Rates

The sedimentation rate at each core location was determined using established methods that incorporate naturally occurring and bomb-fallout radio-isotopes, ^{210}Pb and ^{137}Cs, respectively (e.g., Ketterer et al., 2003; Wilson et al., 2005).

The ^{137}Cs in North American soils resulted from atmospheric testing of nuclear weapons during the 1950s and 1960s. Atmospheric deposition of ^{137}Cs began in 1952 with the onset of atmospheric, atomic bomb testing, peaked in 1964, and has been negligible since the early 1980s (Ritchie and McHenry, 1990). Even though ^{137}Cs is no longer being deposited atmospherically, it is still present in the soil column due to its 30-year half-life. As a result of the incredibly large scale of the nuclear testing conducted from 1952 to 1964 the historical fallout pattern of ^{137}Cs is well defined. The 1964 fallout peak provides an excellent marker for dating sediments in depositional areas.

Once in the atmosphere, the radionuclides attached to aerosols and were delivered to the landscape primarily with precipitation (e.g., Ritchie and McHenry, 1990; Todd et

al., 1989). The radionuclides readily absorbed to soil particles upon reaching the landscape due to high partition coefficients ($K_d \sim 10^4$ to 10^6; e.g., Robbins et al., 1979; Balistrieri et al., 1984). They remained attached to the eroded particles as they traveled into local streams and eventually to a catchment.

In order to determine sedimentation rates using ^{137}Cs, the distance down core is measured to the peak activity of ^{137}Cs. This peak activity corresponds to the maximum delivery in 1964. Thus, the vertical distance corresponds to the amount of material deposited since 1964 (Ritchie and McHenry, 1990).

The naturally occurring radionuclide, ^{210}Pb, is a daughter in the ^{238}U-decay series. The ^{238}U ($t_{1/2} = 4.5 \times 10^9$ years) in soils decays through a series of daughters to gaseous ^{222}Rn ($t_{1/2} = 3.83$ days). A portion of the ^{222}Rn remains in situ, while some of it diffuses into the atmosphere. The ^{222}Rn in the soil and the atmosphere further decays to ^{210}Pb through a series of short half-lived daughters. The ^{210}Pb produced from the ^{222}Rn in the soils is termed "supported ^{210}Pb". (The activity of this supported ^{210}Pb was determined from the activity of the ^{214}Bi parent.) The ^{210}Pb produced from the ^{222}Rn in the atmosphere is termed "excess ^{210}Pb" (Walling et al., 2003). Once in the atmosphere, the excess ^{210}Pb attaches to aerosol particles and is delivered similarly to ^{137}Cs.

Sedimentation rates using ^{210}Pb are determined with either the Constant-Initial-Concentration (CIC) or Constant-Rate-of-Sedimentation (CRS) method (Shukla, 1996). The CIC method assumes that the concentration of excess ^{210}Pb in the depositing sediment is constant at all times. The CRS method assumes that the flux of excess ^{210}Pb in the depositing sediment is constant at all times.

Figure 3.1: Map of Alaska Depicting Black Lake (Google Earth Pro, 2011)

Figure 3.2: Map of Black Lake Depicting Tributaries (Google Earth Pro, 2011)

Figure 3.3: Sample Extraction Methods

A) Manually Pounding Core into lake bed
B) Sealing Core Tube to Create Vacuum
C) Alternative Method for vacuum creation

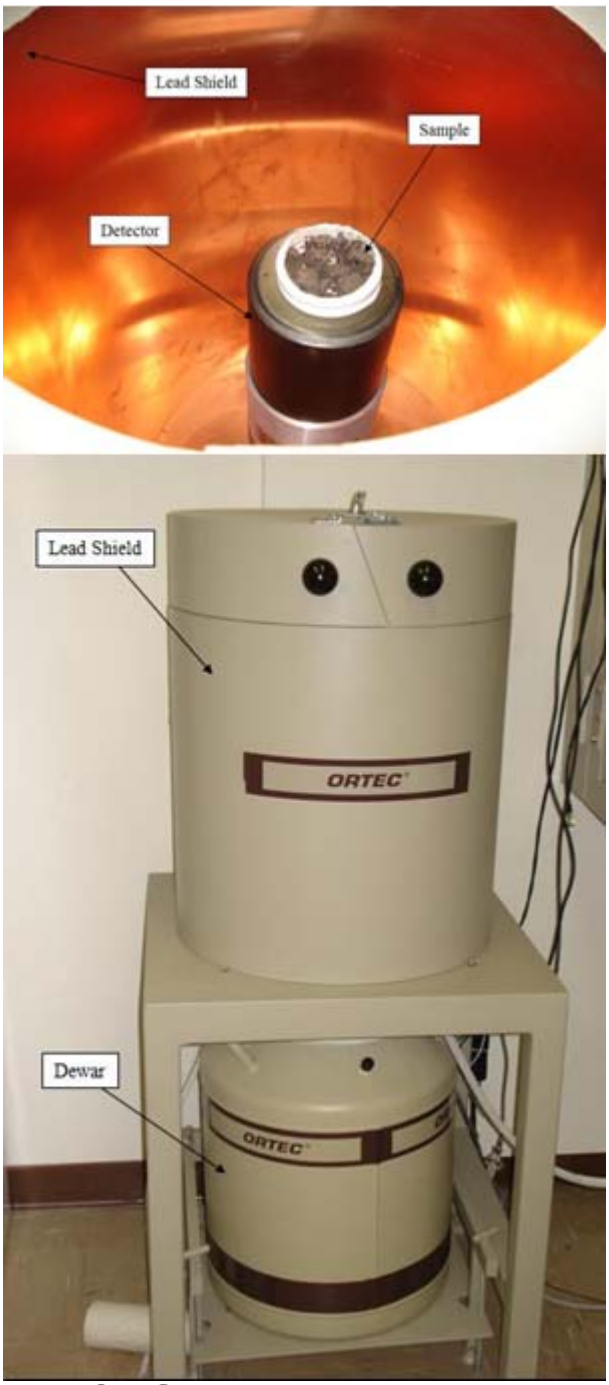

Figure 3.4: Gamma Detector at IIHR - Hydroscience and Engineering, Iowa City, IA

CHAPTER 4: RESULTS

4.1 Introduction

This section outlines the results of this study including (1) the description of the sediment texture characteristics at the sampling locations shown in Figure 4.1 and Figure 4.2 is provided (2) grain size distribution for each core, and (3) the depth-activity profiles of ^{137}Cs are provided for those selected locations.

In order to adequately evaluate other aspects of the Black Lake system, its unique characteristics and geometry must first be evaluated. As described in Elhakeem and Papanicolaou (2008), the surface area of Black Lake is approximately 43 km^2, which classifies it as a small to intermediately sized lake. In catchments of this scale the distribution of incoming sediment is heavily dependent on the locations of the tributaries and the lake outlet. In contrast, lakes of intermediate to large size classifications are generally influenced by wind and strong recirculation patterns. This phenomenon was noted during a study that examined resuspension and hydrodynamics in Lake Okeechobee, FL (Jin and Sun, 2007).

Another area of concern in understanding the hydraulics of Black Lake is its trapping efficiency. As Elhakeem and Papanicolaou (2008) found through numerical modeling and experimentation performed in Black Lake, its trapping efficiency is nearly 92% under a wide range of flow conditions. This suggests that the Black Lake watershed (e.g. the Alec River, Black Lake, and the Black River) can be treated as a closed system, and therefore the use of radionuclides, such as ^{137}Cs, is possible in determining depositional budgets and sedimentation rates. As noted in the methodology chapter of

this thesis, the use of ^{137}Cs relies on identifying its peak atmospheric deposition, which took place in 1964 as a result of large scale, atmospheric, atomic, bomb testing (Ritchie and McHenry, 1990). In addition to the 1964 peak a second peak is sometimes found higher in the soil column relating to the accidental release of ^{137}Cs during the Chernobyl nuclear facility meltdown in April 1986. In addition to identifying the cesium peaks, this method also relies on the quick removal of ^{137}Cs from the water column in lakes via its sorption to sinking suspended sediment particles. For example, 75% of the Chernobyl fallout of radio-cesium deposited immediately following the meltdown was removed from the water column by November 1986 through settling (Santchi et al., 1988). Due to its being a closed system, and that its high trapping efficiency will lend itself to high degrees of particle sorption, it is safe to suggest that ^{137}Cs can be utilized to accurately estimate the sedimentation rates in Black Lake, which are the center piece of this thesis.

4.2 Texture Analysis

The success of using activity profiles of ^{137}Cs to determine sedimentation rates is strongly dependent on sediment composition. The presence of clay and silt is critical for sorption of ^{137}Cs to sediments (He and Walling, 1996), and therefore is required for its detection within the sediment profile. For this reason, Figure 4.3 depicts sub-samples extracted from the following core locations: A1, along the sand spit near the South Fork (SF) delta; A2, also along the sand spit; A4, at the fork of the Alec River; and the lake outlet. The sediment at the spit, exhibits a dark color when it is compared to the sediment at the outlet, which is characterized by a light brown color. Upon visual inspection, the sediment at this location has little chance of mobilization, or resuspension, due to the high percentage of coarse sand particles present. Although the nature of this comparison

is rather qualitative, there is a strong indication that samples at A2 contain large amounts of organic material relative to the samples at the outlet. This comparison is further substantiated when the radioactivity at the two sites are compared. Select activities of ^{137}Cs from the spit are slightly higher than activities of ^{137}Cs at the outlet, since ^{137}Cs easily bonds to organic matter (Agapkina et al., 1995).

In order to demonstrate the changes in sediment delivery and sedimentation rates, visual analysis was also performed on samples from the North and South Forks of the Alec River (Figure 4.4) Flow in the NF has recently diverted to form a new channel (Figure 4.5) in addition to the original channel (Ruggerone, 2003). Pictures of sub-samples are provided for the newly re-routed North Fork channel and the "old" North Fork channel (hereafter referred to as NF New and NF Old, respectively) over the course of the last 15 years. The remnants of this diversion are well illustrated by the soil texture, shown in Figures 4.4b and 4.4e. Figure 4.4e shows patches of finer material distributed throughout the sample. The sample pictured in Figure 4.4b shows a lack of fine material and is characterized by a coarse, granular texture.

Due to the inlets playing such an important role in a small, closed system, samples were also taken from the following four tributaries: Canoe, Cottonwood, Crooked, and Linhome Creeks (Figure 3.2). The differences in color and size distribution of the samples are notable (Figure 4.6). Samples extracted from Crooked and Linhome Creeks are highly organic; a substantial amount of roots and small sticks was visible in both samples. The Canoe Creek sample was less organic, where the Cottonwood Creek sample indicated the presence of tephra, which is material derived from the volcanic activity of nearby Mount Veniaminof. In a study conducted in the early 1990s (Stihler et

al., 1992) the presence of tephra in sediments of this region, through a tephrochronological study, was discovered. This corroborates the visual observation of tephra at the Cottonwood Creek site (Figure 4.4c).

In summary, the above textural analysis reveals that wide spectrums of sediment size and composition exist within Black Lake. These distinct size variations may help to determine sedimentation rates at the inlet and outlet locations, as well as verify the results of the ^{137}Cs profile analysis, due to ^{137}Cs readily adhering to silt and clay particles.

4.3 Profiles of ^{137}Cs

The ^{137}Cs profiles shown in Figure 4.7 – Figure 4.15 provide the following two pieces of information: (1) the variations with depth of this anthropogenic radionuclide, ^{137}Cs, and (2) the fine material distribution of each location. The depth profiles of ^{137}Cs for the selected core sites show one major peak, which correlates to the maximum atmospheric ^{137}Cs deposition peak from 1964 described above. No secondary peaks were observed, indicating no observable contribution from the Chernobyl incident. Despite the variability that may exist with the delivery of ^{137}Cs from the surrounding landscape to the lake (e.g., water recirculation and mixing), Figures 4.5 – 4.13 can be used to date the sediment and obtain sedimentation rates at each core location (Porto et al., 2001), which is the overarching goal of this study. The sedimentation rates, determined with activities of ^{137}Cs were compared against the computational results presented by Elhakeem and Papanicolaou (2008). In addition, the analysis of sedimentation rates using ^{137}Cs was complemented with the ^{210}Pb derived sedimentation rates, as described in the methods chapter of this thesis. However, the variability and complexity observed in the occurrence of ^{210}Pb was too high to determine adequate sedimentation rates using that isotope. This

can be attributed to the geographical location of Black Lake, namely on the Alaskan Peninsula. Rain events, which are the primary delivery mechanism of atmospheric ^{210}Pb, travel over many miles of open water before arriving over the Black Lake watershed. Since the source of atmospheric ^{210}Pb is ^{238}U, which is predominantly found in landscape soils, the rain events over Black Lake are depleted of ^{210}Pb making it impossible to determine sedimentation rates using this source. For this reason, no ^{210}Pb rates are presented in this thesis.

The activity profiles of ^{137}Cs (Bq/g) versus the depth (cm) illustrate striking differences between the deposition rates occurring between the outlet and NF Old with the remaining sampling locations (Figures 4.5– 4.13). In the former case of the outlet and NF Old, the peak activity of ^{137}Cs occurs roughly 22 cm below the current bed surface, whereas in the later case, the peak activity of ^{137}Cs occurs, on average, at 7 cm below the current bed surface. When these peak values are divided over the period since 1964 (46 years), the annual average sedimentation rates in cm/yr, which summarized in Table 4.1, can be determined. The differences noted in the sedimentation rates at the NF Old and outlet sites can be explained from hydrologic and sedimentologic points of view. Figure 4.5 clearly show the diversion of the channel of the Alec River from the old channel to the new channel (Buffiington, 2002). It is thought that during the period corresponding to the evolution of the NF New channel, water and fine sediment still occasionally flowed into the NF Old channel. During that period, the flow in the NF Old channel was relatively stagnant when compared to the newly evolved NF New channel. As a result, the likelihood of increased sedimentation for fine material found within the old channel was high compared to the NF New channel where shear flow action tended to keep the

finer material in suspension. This means that sediment from the NF New channel is more likely to remain suspended, and thus more likely to be deposited in Black Lake.

A similar process to that shown in the North Fork is speculated to have occurred at the outlet of the lake. This is further evidenced when the wide historical variability in the Black Lake sedimentation is examined. As several studies by Ruggerone (1994, 2003), Buffington (2002), and Elhakeem and Papanicolaou (2008) have noted, the lake outlet experienced significant deposition in the late 1950s and early 1960s. Another shift in the depositional patterns observed at the lake outlet occurred in the 1970s. At that time, the outlet of the lake experienced large scale degradation, which resulted in a widening of the outlet and the formation of a headcut (i.e., drop in bed elevation). The above studies attributed the degradation at the outlet to volcanic activity and high sediment delivery through the West Fork, which empties into the Black River below the lake. In other words, West Fork behaved as a control point due to significant deposition occurring at the confluence between West Fork and the Black River (Figure 4.16 and Figure 4.17). This control point created a bottleneck for the incoming flow resulting in backwater effects upstream of the confluence and, as a result, sediment starvation. Due to the lack of sediment supply, the drop in bed elevation at the outlet of the lake was intensified. As recently as summer 2010, this drop was measured to be nearly 3 m. Simply put, during the last quarter of the 20th Century, deposition occurred at the lake outlet, as expected, however, external factors acting on the Black Lake system (e.g., West Fork and volcanic activity at Mount Veniaminof) have resulted in significant bed degradation at the lake outlet.

These explanations verify the distributions and peak activities of ^{137}Cs observed in at locations NF Old and the Outlet, Figure 4.9 and Figure 4.8, respectively. At NF Old and the lake outlet, the peak activities of ^{137}Cs are below the top 10 cm of the cores, which is indicative of significant deposition of fine material taking place since 1964. These results are in contrast to the peak activities of ^{137}Cs shown in the remaining figures, as they are are found within the top 10 cm of each sample. This indicates that less deposition occurred in those locations since 1964. This is reasonable considering that most of these locations are located at the outlets of the tributary locations and the North and South Forks of the Alec River. Field surveys conducted in August 2010 support these findings.

In addition to the activity distributions versus depth, the silt and clay percentages at the sampling locations are presented. In most locations, other than the NF New and SF Down, the percentage of fine material is relatively high, 60% or higher. The high percentages of sand at the NF New and SF Down locations coincide with the delta depositional patterns observed during the field survey conducted in summer 2010.

In addition to the variability of soil type, there are a variety of reasons for the differences in the distributions of ^{137}Cs values found at the different sampling locations. These differences have to do with water circulation patterns and residence times of particles within the lake. These variables may have affected the distribution of ^{137}Cs over time. However, dispersion analyses used to identify areas with heavy mixing were not completed as part of this study. These results, along with the results of Elhakeem and Papanicolaou, 2008, seem to suggest that, flow exiting from the South Fork of the Alec

River flow directly to the lake outlet and the Black River, rather than circulating within Black Lake itself.

Another element of Figures 4.5 – 4.13 is that the depth at which the activity of ^{137}Cs goes to zero is clearly illustrated. This depth corresponds to the year 1952, the first major year of atmospheric atomic bomb testing. The peak and zero activities of ^{137}Cs from each location will be used to determine the sedimentation rates following the procedure outlined in Chapter 3. These sedimentation rates are summarized in Table 4.1. Other than the magnitude of sediment at the Canoe River sampling location, there is little difference between estimates of the sedimentation rates using the two benchmark dates. The spatially averaged sedimentation rate for these two benchmark dates are 0.25 cm/yr.

The findings of this study were compared against the numerical experiments of Elhakeem and Papanicolaou (2008), where the volume of sediment entering the lake per day was estimated at nearly 20 m^3. Yearly, this volume results in 7300 m^3 entering the lake. Taking into consideration that the trapping efficiency of the lake is 92% (Elhakeem and Papanicolaou, 2008), this leads to 6716 m^3 of sediment depositing in the lake. When the total surface area of lake is considered, which is 43 x 10^6 m^2, then the estimated, spatially averaged deposition rate is 0.16 cm/yr. Elhakeem and Papanicolaou (2008) did not consider any contributions from the four tributaries. Thus, the estimates derived by the ^{137}Cs analysis compares extremely well with this sediment budget from their study. The ^{137}Cs analysis reveals additional information that the numerical information could not provide, namely the spatial distribution of the depositional patterns within the lake. Using the ^{137}Cs technique, the areas of heaviest sedimentation since 1964 can be located.

Finally, in order to further verify the results of this study, the sedimentation rates observed in Black Lake are compared with sedimentation rates determined using the ^{137}Cs approach in geographical areas found in close proximity to Black Lake (i.e., in Alaska). In Smeaton Bay near Juneau, AK, deposition rates determined via ^{137}Cs ranged between 0.24 - 0.36 cm/yr (Sugai 1990). In another study in Skilak Lake, AK (Stihler et al. 1992), sedimentation rates were found to be between 0.03 – 0.13 cm/yr using ^{137}Cs. Although those systems have experienced different natural and anthropogenic activities, these qualitative comparisons show the relative uniformity of this method in determining sedimentation rates in systems experiencing similar hydrologic phenomena in Alaska.

Table 4.1: Results For Each Sample Location

Location	Latitude	Longitude	Sediment Depth (cm)	Rate Since 1952 (cm/yr)	Rate Since 1964 (cm/yr)
A4	56°27'17.10"N	158°55'46.90"W	21.25	0.37	0.46
Outlet	56°24'46.20"N	158°56'23.28"W	23.75	0.41	0.52
North Fork (New)	56°28'6.30"N	158°55'53.30"W	16.25	0.28	0.35
North Fork (Old)	56°28'9.30"N	158°55'47.00"W	21.25	0.37	0.46
North Fork Delta Up	56°27'57.40"N	158°55'49.20"W	6.25	0.11	0.14
South Fork Down	56°26'35.10"N	158°56'49.30"W	8.75	0.15	0.19
South Fork Delta Up	56°26'42.80"N	158°56'16.40"W	6.25	0.11	0.14
Canoe Creek	56°28'48.00"N	159° 3'54.80"W	3.75	0.06	0.08
Crooked Creek	56°27'8.90"N	159° 3'34.60"W	8.75	0.15	0.19

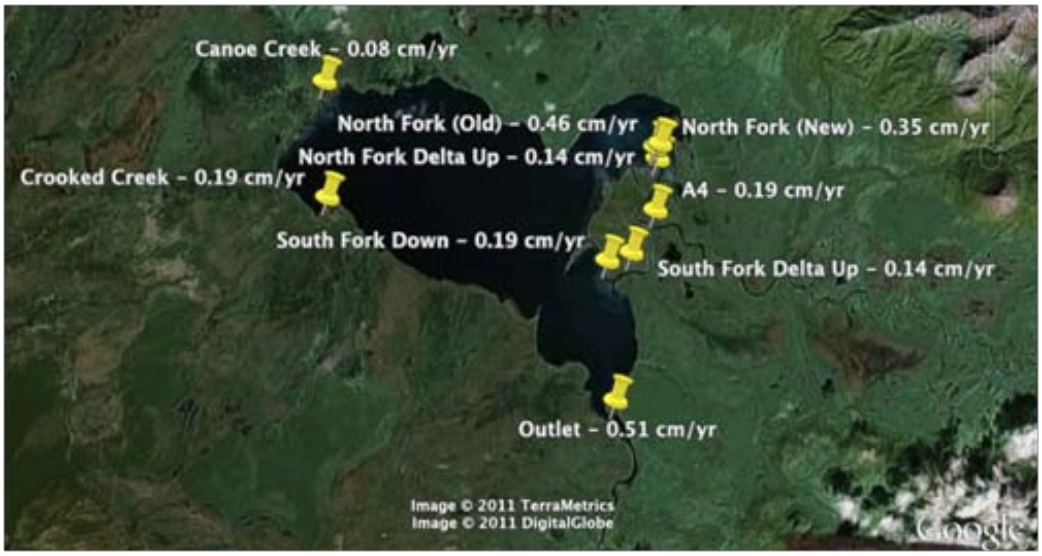

Figure 4.1: Map of Black Lake Depicting Sample Locations and Sedimentation Rates (Google Earth Pro, 2011)

Figure 4.2: Map of North Fork Delta Depicting Specific Sample Locations and Sedimentation Rates (Google Earth Pro, 2011)

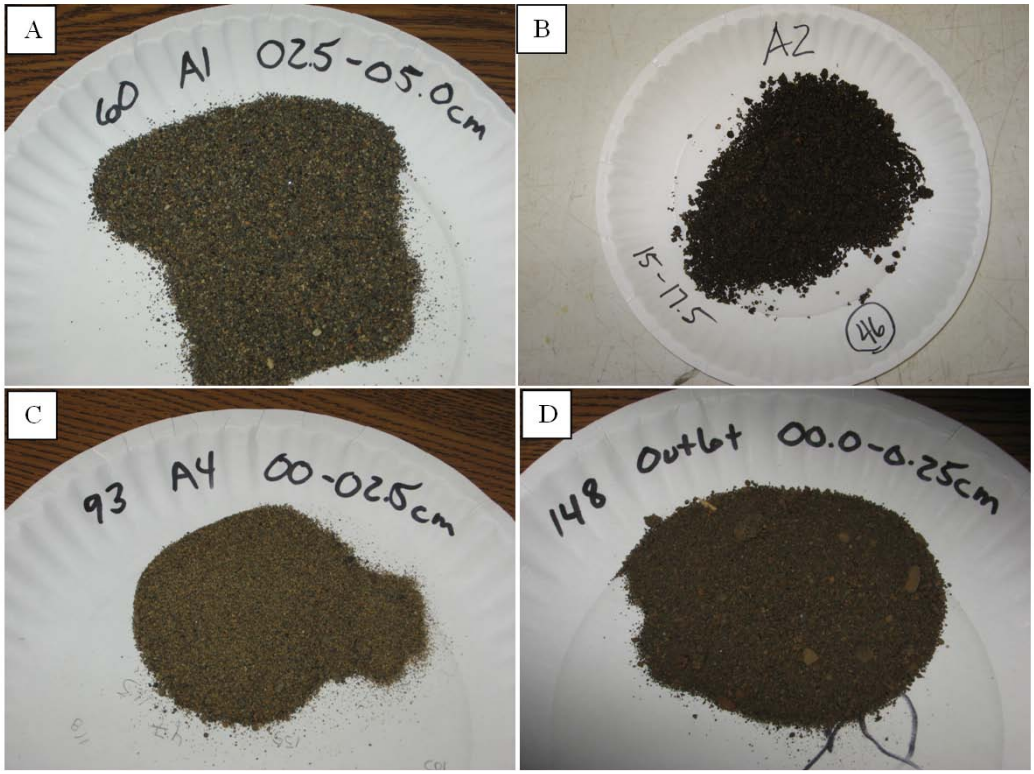

Figure 4.3: Sample Pictures from the Sand Spit and Outlet

A) Sample 60: A1 (2.5 – 5.0cm)
B) Sample 46: A2 (15.0 – 17.5cm)
C) Sample 93: A4 (0.0 – 2.5cm)
D) Sample 148: Outlet (0.0 – 2.5cm)

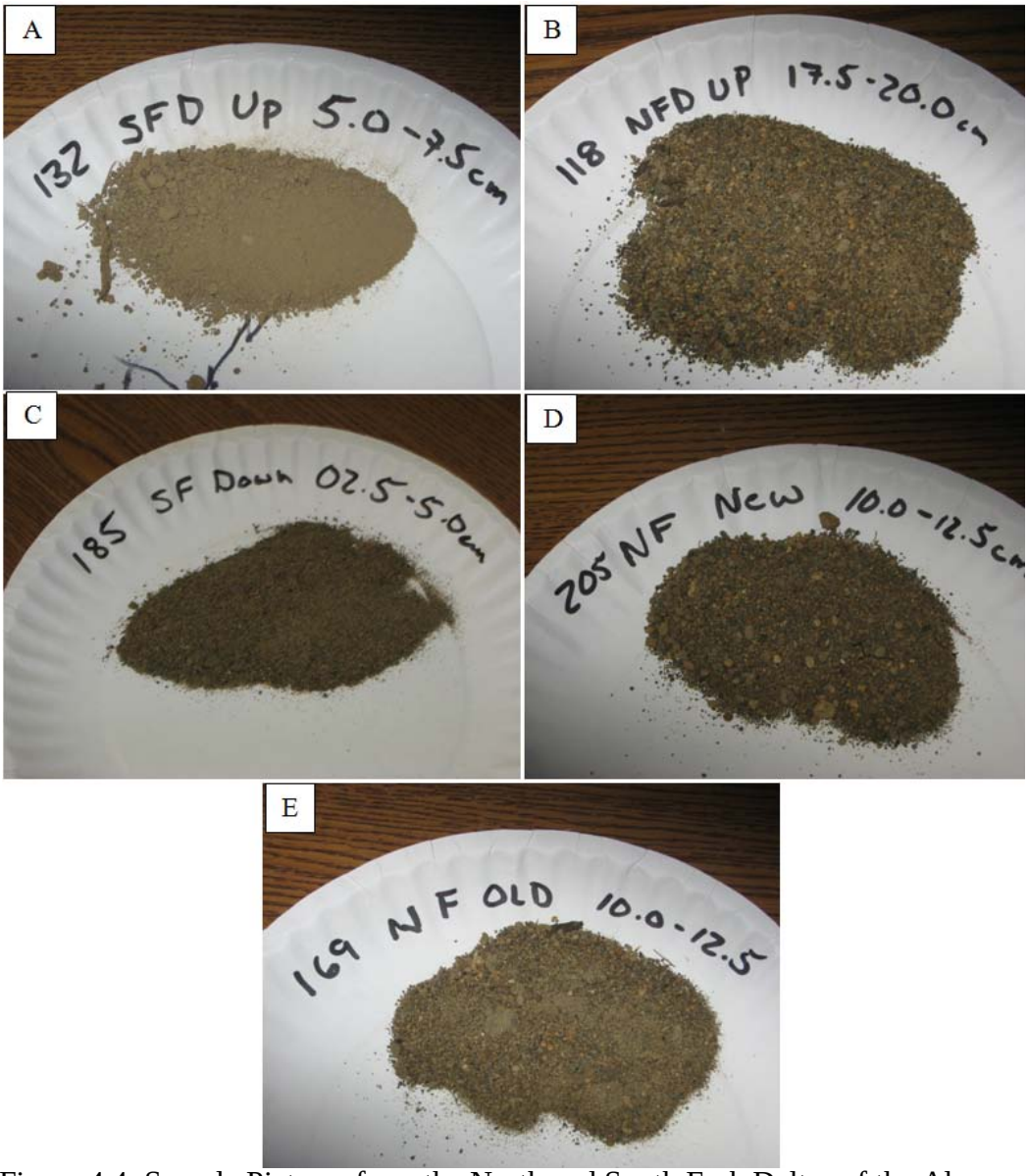

Figure 4.4: Sample Pictures from the North and South Fork Deltas of the Alec River

A) Sample 132: SFD Up (5.0 – 7.5cm)
B) Sample 118: NFD Up (17.5 – 20.0cm)
C) Sample 185: SFD Down (2.5 – 5.0cm)
D) Sample 205: NF New (10.0 – 12.5cm)
E) Sample 169: NF Old (10.0 – 12.5cm)

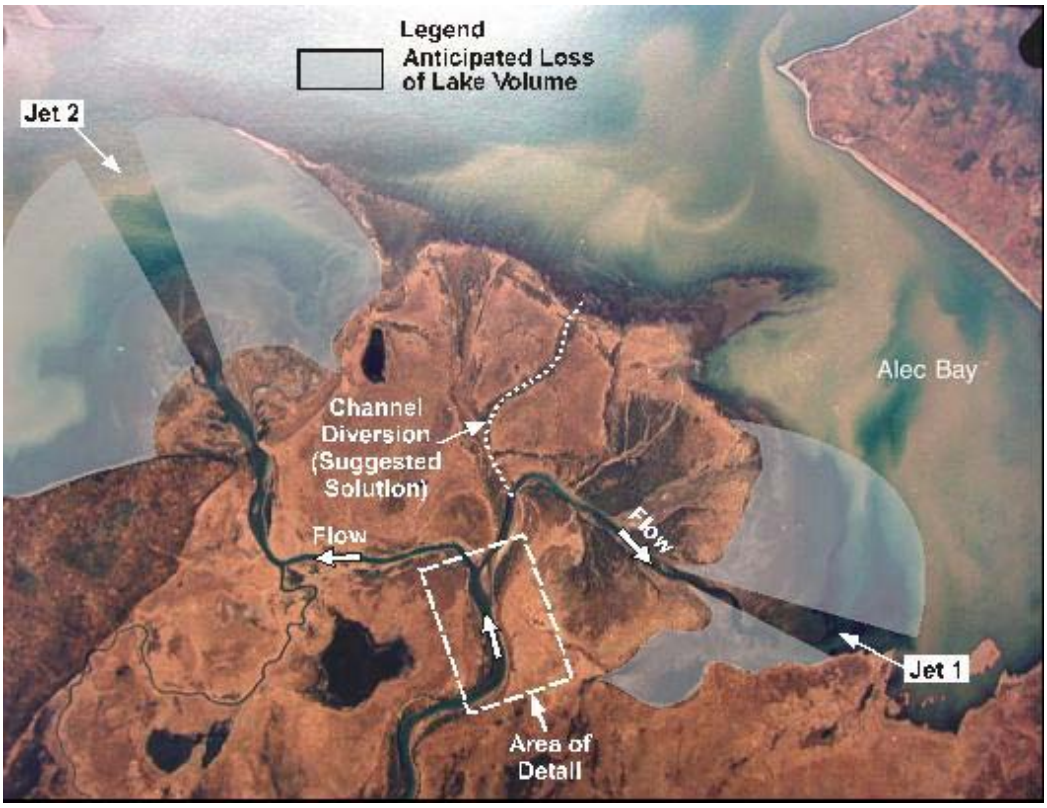

Figure 4.5: North Fork Delta Showing New and Old Channels

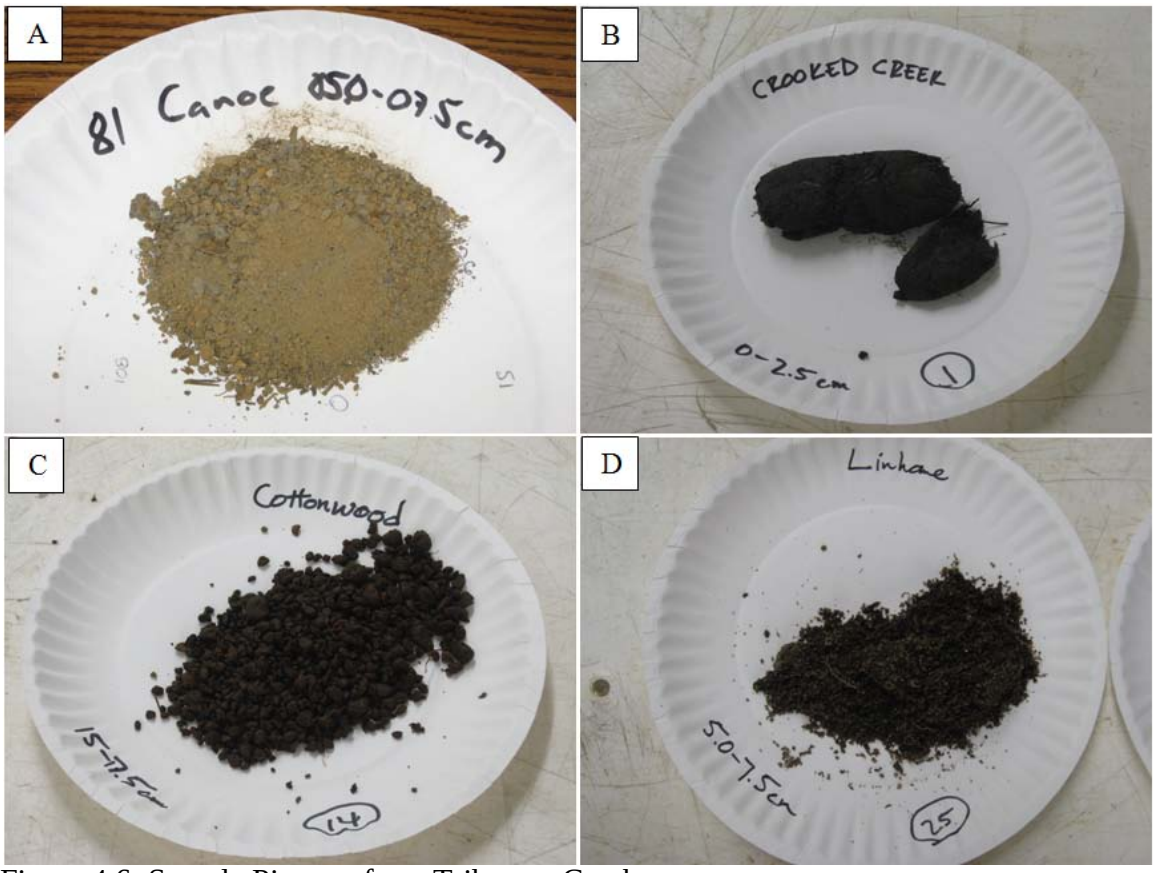

Figure 4.6: Sample Pictures from Tributary Creeks

A) Sample 81: Canoe (5.0 – 7.5cm)
B) Sample 01: Crooked (0.0 – 2.5cm)
C) Sample 14: Cottonwood (15.0 – 17.5cm)
D) Sample 25: Linhome (5.0 – 7.5cm)

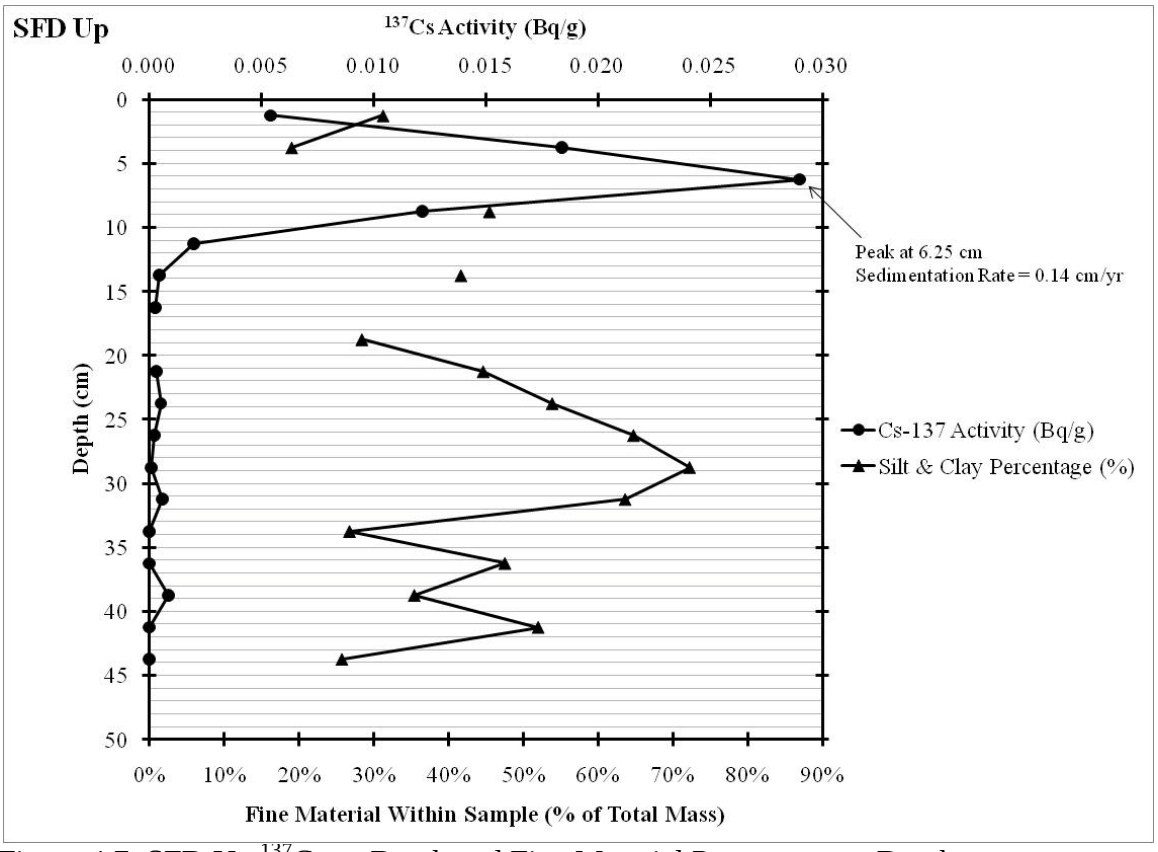

Figure 4.7: SFD Up ^{137}Cs vs Depth and Fine Material Percentage vs Depth

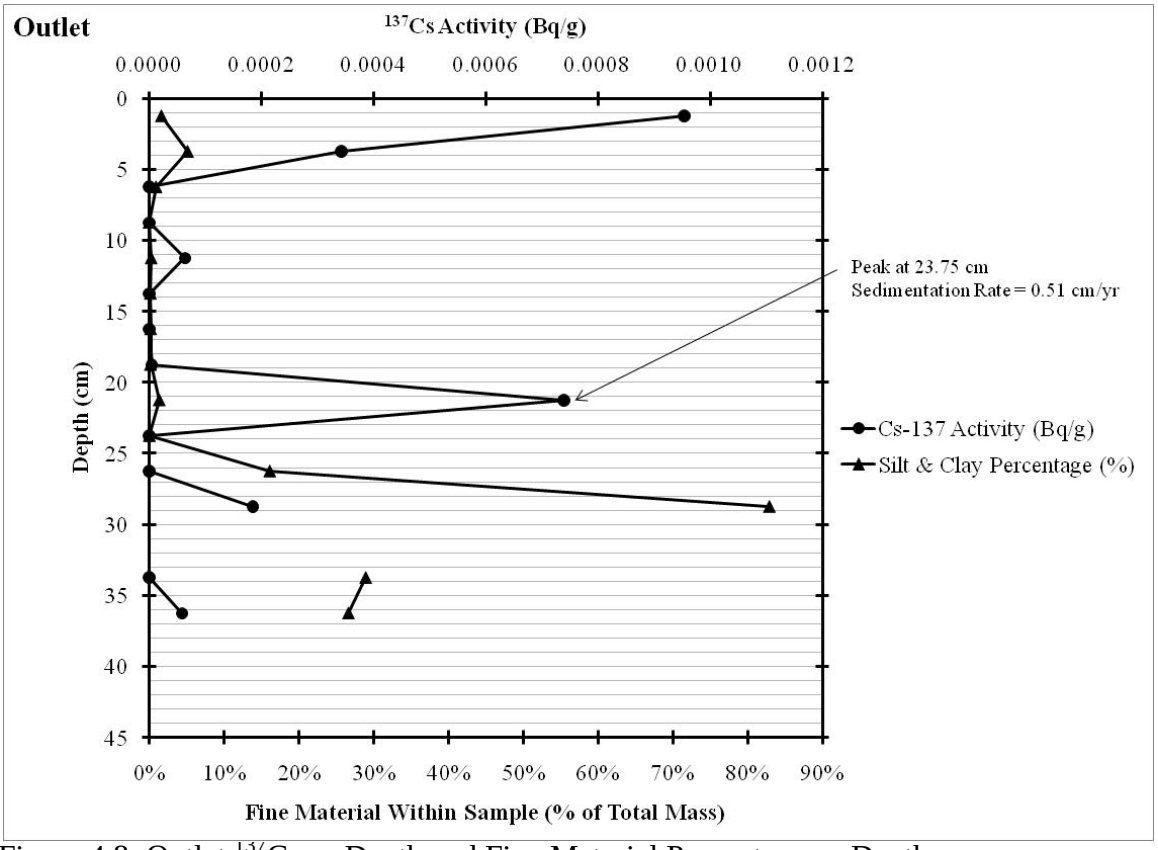

Figure 4.8: Outlet ^{137}Cs vs Depth and Fine Material Percentage vs Depth

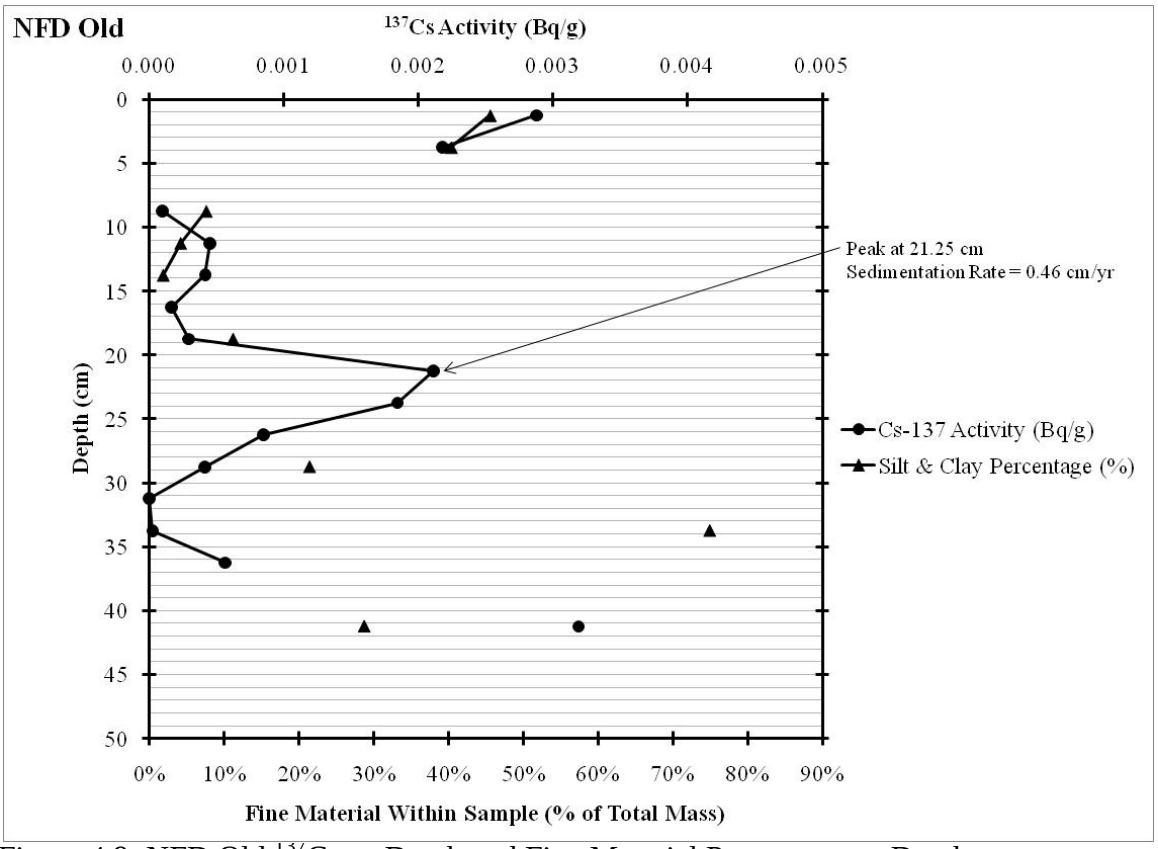

Figure 4.9: NFD Old ^{137}Cs vs Depth and Fine Material Percentage vs Depth

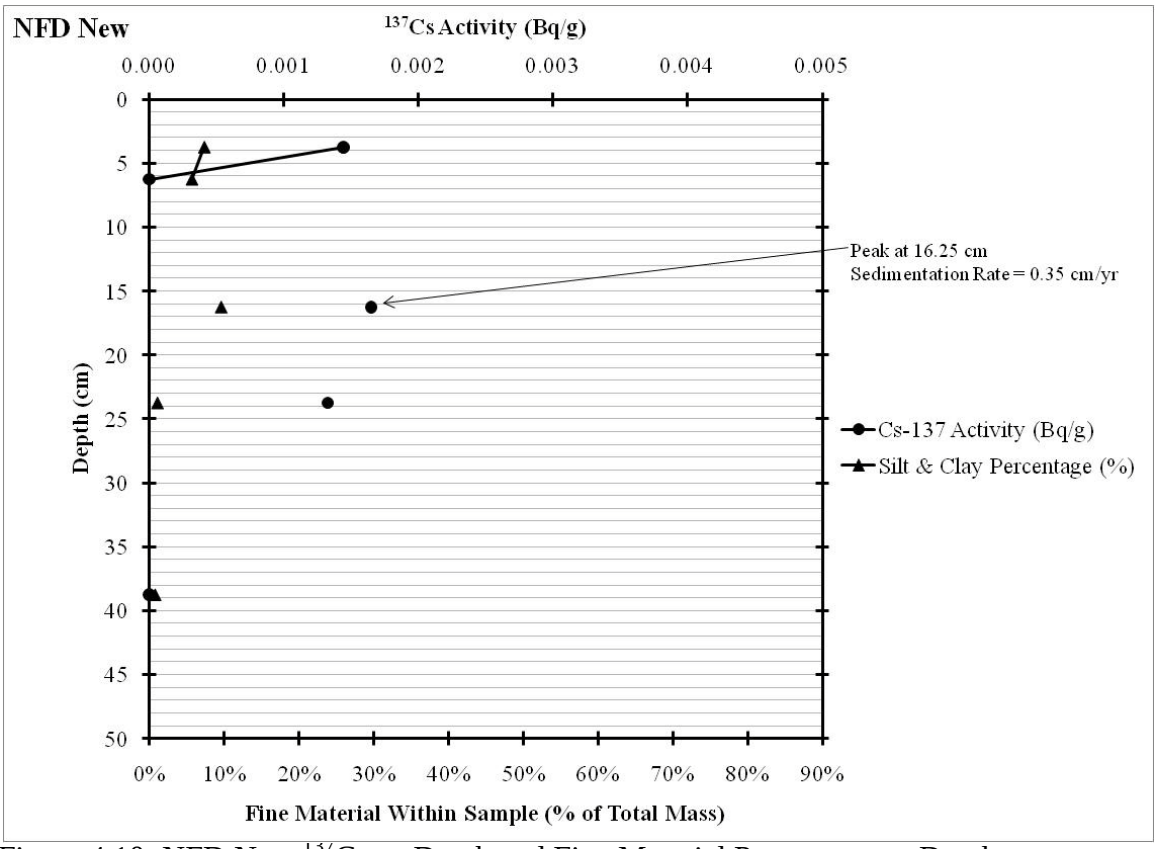

Figure 4.10: NFD New ^{137}Cs vs Depth and Fine Material Percentage vs Depth

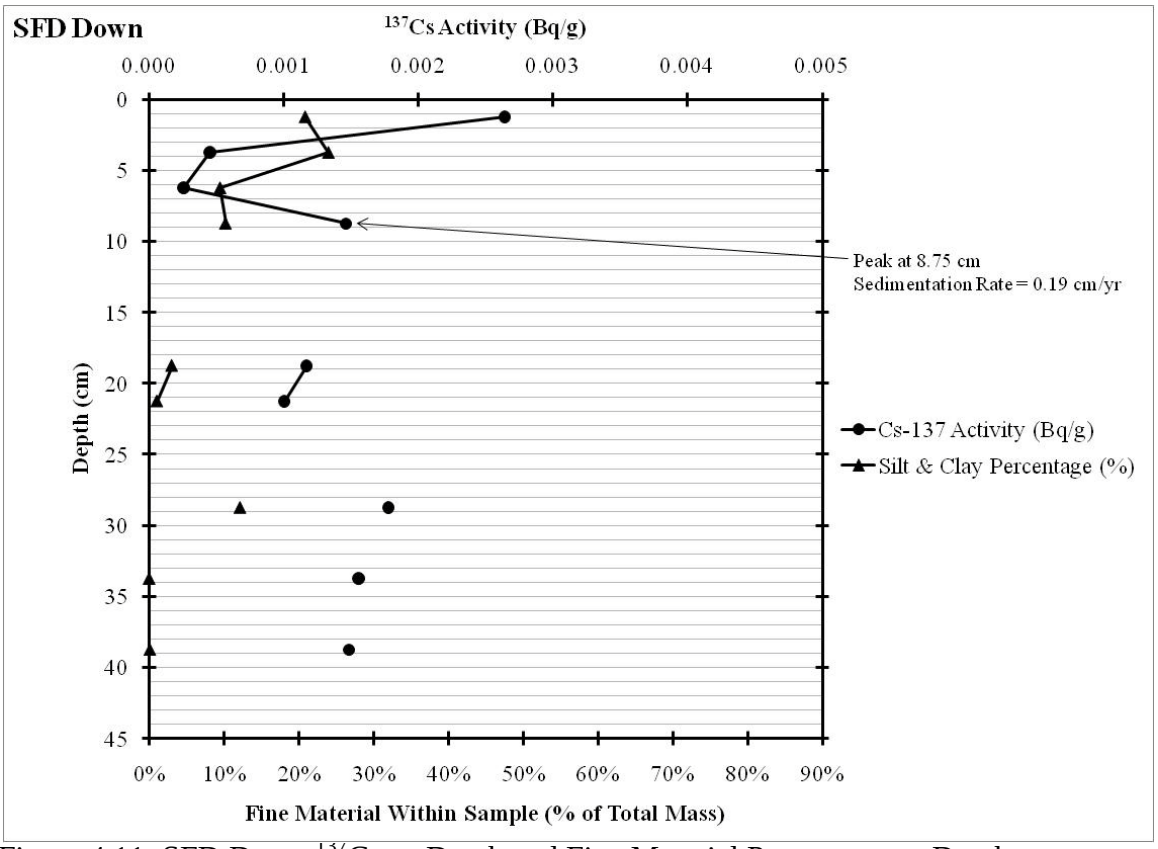

Figure 4.11: SFD Down ^{137}Cs vs Depth and Fine Material Percentage vs Depth

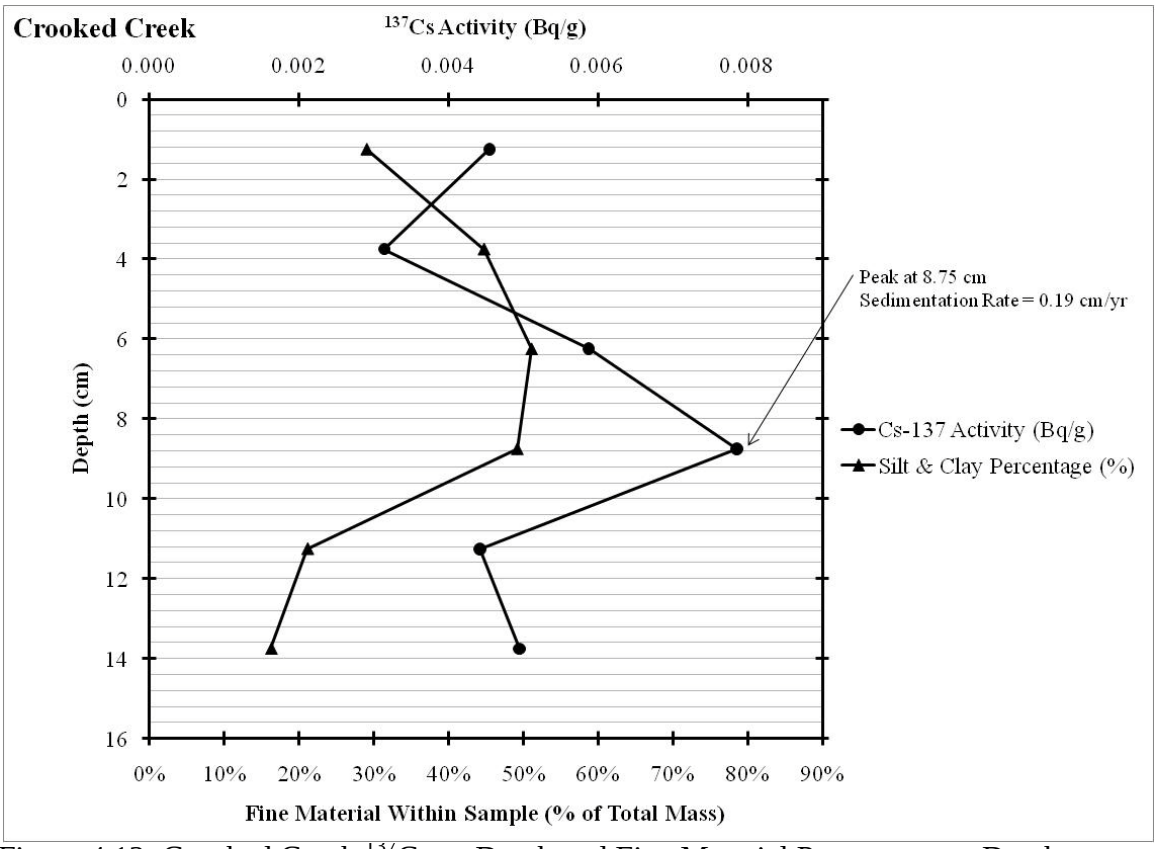

Figure 4.12: Crooked Creek ^{137}Cs vs Depth and Fine Material Percentage vs Depth

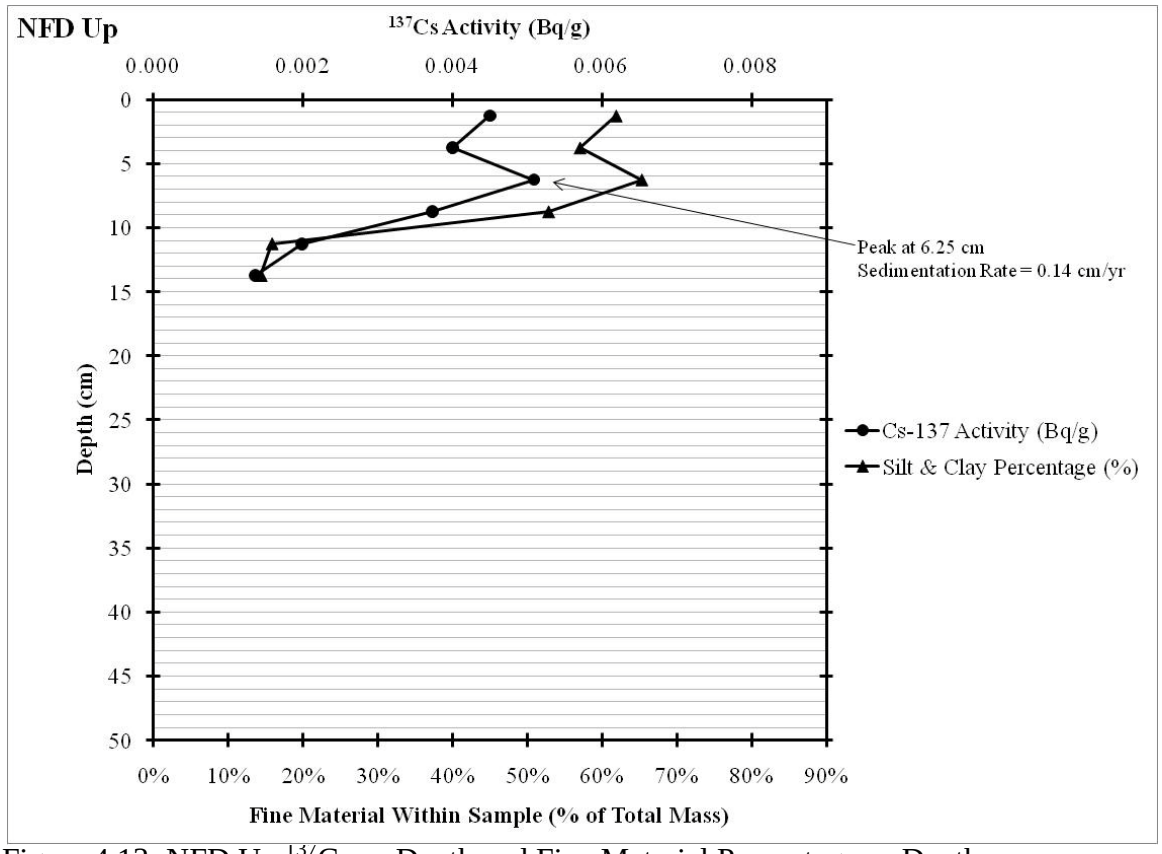

Figure 4.13: NFD Up ^{137}Cs vs Depth and Fine Material Percentage vs Depth

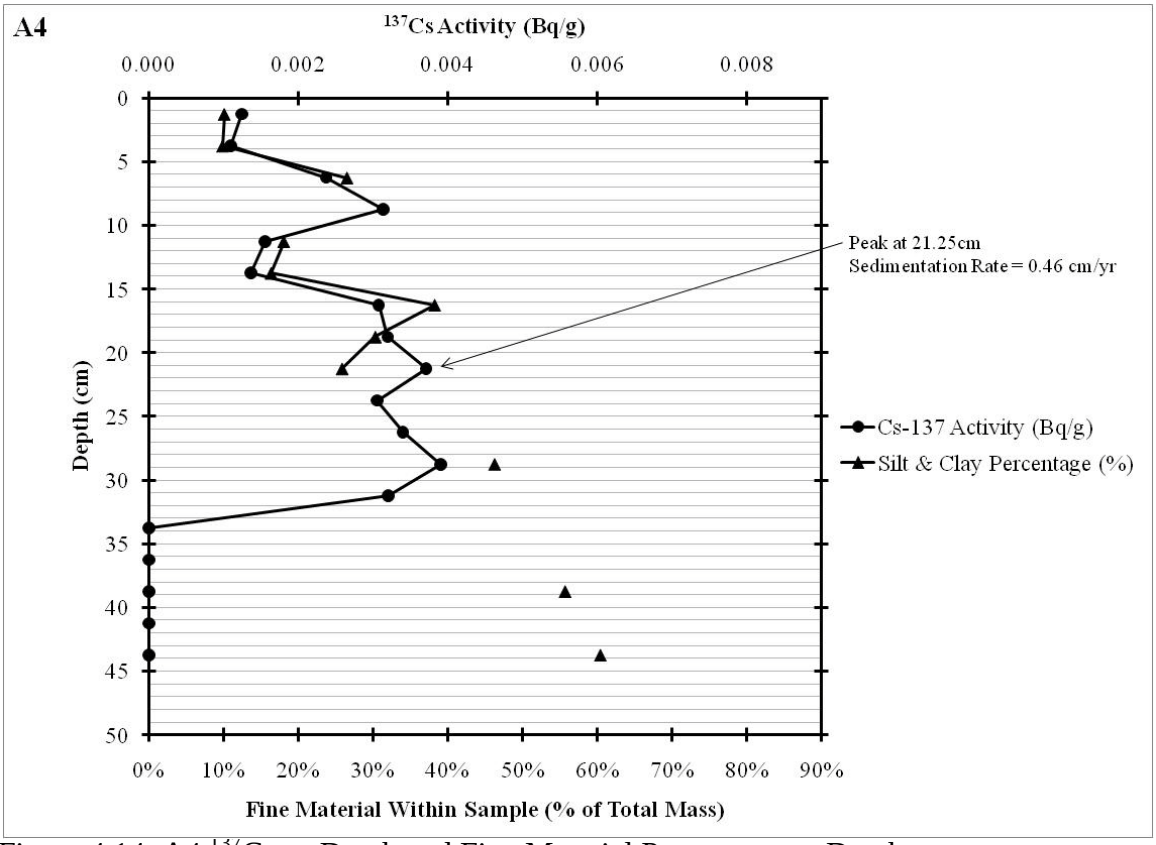

Figure 4.14: A4 ^{137}Cs vs Depth and Fine Material Percentage vs Depth

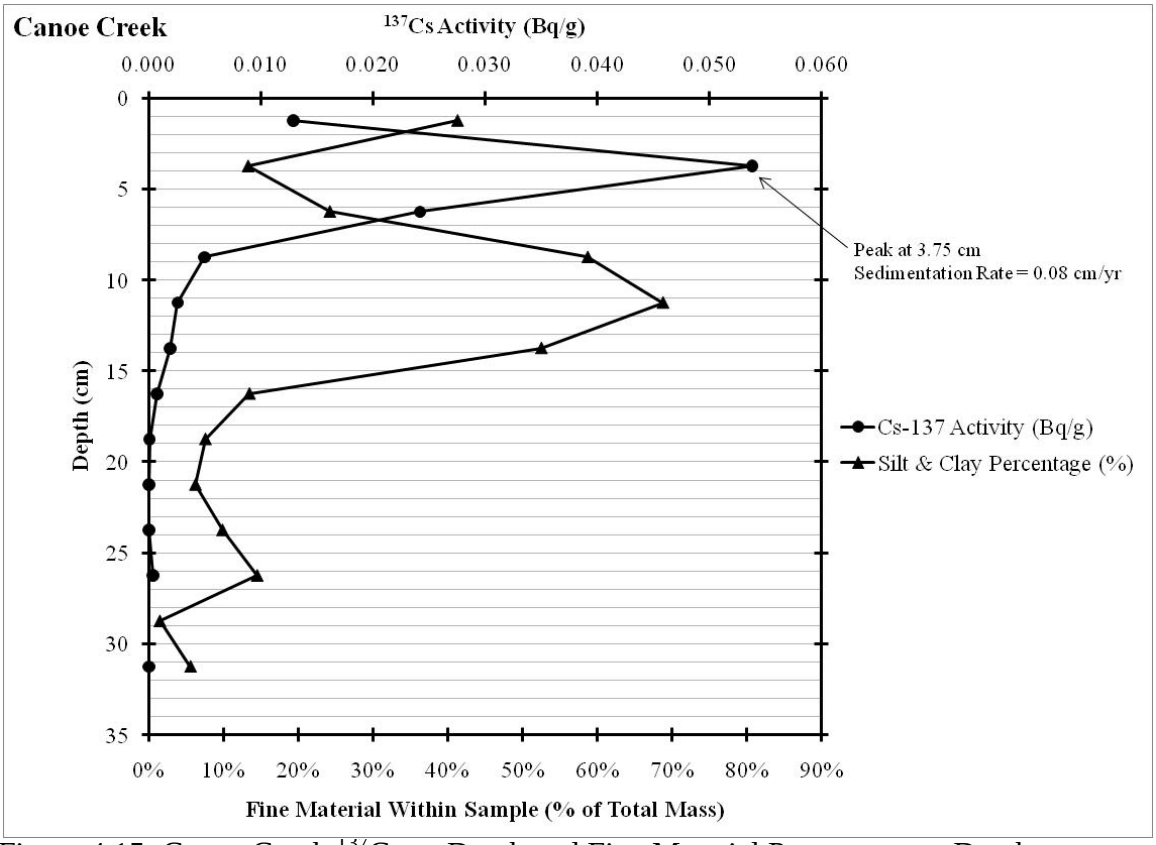

Figure 4.15: Canoe Creek ^{137}Cs vs Depth and Fine Material Percentage vs Depth

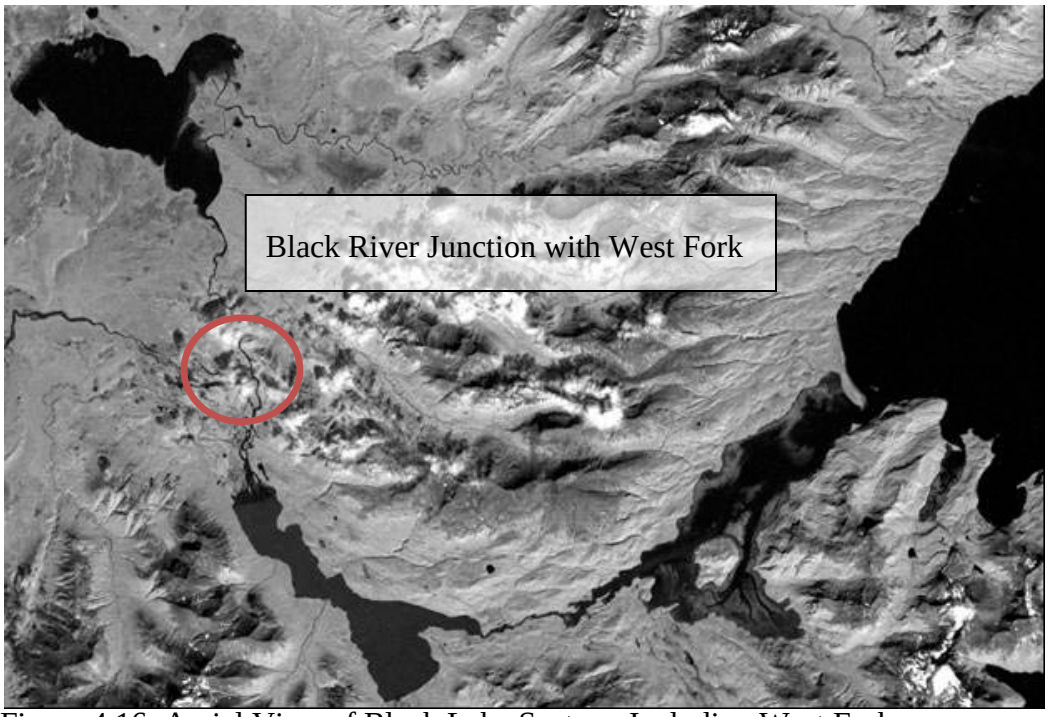

Figure 4.16: Aerial View of Black Lake System, Including West Fork

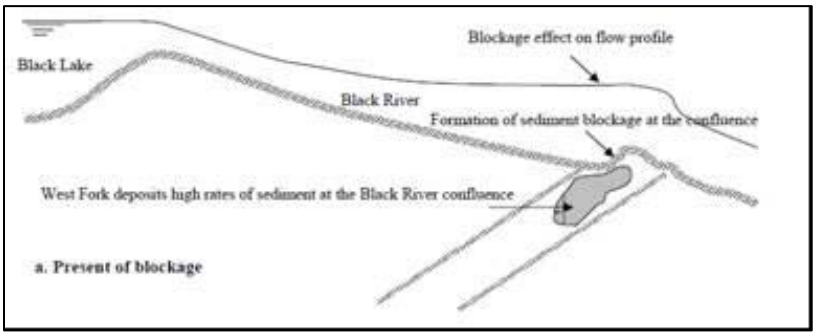

Figure 4.17: Black Lake System Stick Model

CHAPTER 5: CONCLUSIONS

5.1 Project Summary

This study provided, quantitatively, the sedimentation rates in a lake located on the Alaskan Peninsula, in close proximity to the active volcano Mt. Veniaminof. This region has experienced significant hydrologic fluctuations, which have led to channel migration on the Alec River and increased influxes of sediment in the Black Lake system. Past research in this geographically isolated region has been, at best, qualitative. Currently, there are no systematically obtained data, namely hydrologic and sedimentologic. Past work has put great emphasis on fish counts and temperature models to simulate the end effects of climatic shifts on overall lake water quality. This research aimed to tackle two issues associated with Black Lake. It (1) focuses on the sedimentologic features associated with the lake system and (2) utilizes a state of the art technology, radionuclide tracers, to provide the sedimentation rates in Black Lake.

This work complements the prior numerical study completed by Elhakeem and Papanicolaou (2008) and, at the same time, provides a more complete depiction of the sedimentation rates within Black Lake by accounting for the contributions of the four tributaries: Cottonwood, Canoe, Linhome, and Crooked Creeks. This is the first time these tributaries have been included in a sedimentation study of the lake. By not including these four tributaries the numerical study by Elhakeem and Papanicolaou was able, only, to supply a spatially averaged sedimentation rate over the total surface of the lake. The use of the radionuclides allowed for the determination of the locations that

experience the highest sedimentation rates, and to obtain a chronological assessment of the sediment infilling the lake.

The sedimentologic and radionuclide analyses revealed that most of the material entering the lake is reworked from the beds of the Alec River and the four tributaries. This is evident from the coarser texture of the incoming sediment. However, clayey, silt material has also been found within the depositional areas scattered around the lake. This material was predominantly derived from the uplands and mass failure of the river channel banks. It is not surprising that most of the finer sediment deposits are located near the Alec River North and South Fork Deltas, as these are the areas with the highest composition of fine material. Cottonwood Creek had contributions of tephra, an indication of both volcanic activity and transport of the volcanic material during the snowmelt on Mt. Veniaminof. In addition, some of the tributaries had contributions of finer materials. In contrast, material collected at the outlet of the lake was overpopulated with coarse sediment.

5.2 Results

The sedimentation rates calculated at the sampling locations provided an average sedimentation rate of about 0.25 cm/ yr, which is in close agreement to the spatially averaged rate of Elhakeem and Papanicolaou (2008) and of a study in close proximity to the area, Stihler et al. (1992). Analysis with ^{210}Pb did not produce detectable results and further sampling is needed to conclusively pinpoint areas of sediment provenance using that method. Clearly, the results of this study show that the sedimentation rate is relatively low and support the hypothesis that due to the presence of the spit most of the finer material is directed towards the Black River (Elhakeem et al., 2008). These

observations agree with a visual assessment performed by C.G. Wilson and A.N. Papanicolaou during a field survey in 2010. A clear demarcation was noted between the segment of the lake found in between the South Fork delta and the lake outlet. The water column in that area was full of sediment en route to the Black River. In contrast, the segment of the lake adjacent to the North Fork of the Alec River and Linhome Creek had a water column with much higher clarity.

5.3 Limitations

A primary limitation to conducting this study was the extreme difficulty in performing high quality field research in a location as remote as Black Lake. This alone greatly limits the use of sensors and other equipment that could provide measurements of flow and sediment load at different locations at various times including low and high water events, or during a storm. Involvement of the local community, Chignik Village, in collaboration with other agencies may be the only way of getting around this serious limitation. Transportation of the sensor technology and also any type of construction in the Black Lake system needs to be done with great attention to detail and deep understanding of social, climatic, and financial limitations.

Another limitation of this study is the wide variety of soil types present in the Black Lake system. As has been stated throughout this thesis, radionuclide analysis is possible due to the bonding of isotopes like ^{137}Cs and ^{210}Pb to suspended sediments or very fine particles. As is shown in the high percentages of coarse sand in A1 and A2 this was not always possible. The tephra present in the Cottonwood Creek watershed also

introduces an interesting possibility in testing volcanic sediment using radionuclides in the future.

5.4 Opportunities for Future Research

Future research should utilize a watershed scale model that interconnects the tributaries and the Alec River with Black Lake. Incremental modeling of of the Alec River, or the tributaries alone, will not suffice, and will likely yield inconclusive results regarding the future of Black Lake. As this research has shown, the West Fork is a potential contributor to the degradation of the lake outlet. This is largely due to a substantial influx of material from volcanic activity in the region that has created a bottleneck of deposited sediment. This partial blockage has created a backwater affect, altering the hydraulic regime of the Black River upstream of its confluence with the West Fork.

APPENDIX A: HYDROMETER TABLES

The following tables contain constant values used in hydrometer analysis. The hydrometer analysis procedure is explained in Chapter 3 of this thesis.

Table A.1: Specific Gravity of a Soil Particle Given Temperature

Temperature C	Specific Gravity of Soil Particles				
	2.60	2.65	2.70	2.75	2.80
18	0.014	0.01399	0.0138	0.01359	0.01339
19	0.014	0.01382	0.0136	0.01342	0.01323
20	0.014	0.01365	0.0134	0.01325	0.01307
21	0.014	0.01348	0.0133	0.01309	0.01291
22	0.014	0.01332	0.0131	0.01294	0.01276

Table A.2: Weight Correction Factor (a)

Unit Weight of Soil Solids (g/cm^3)	Correction Factor a
2.85	0.96
2.8	0.97
2.75	0.98
2.7	0.99
2.65	1
2.6	1.01
2.55	1.02
2.5	1.04

Table A.3: Effective Length, L (cm) of Hydrometer Reading

Hydrometer 151H	
Actual Hydrometer Reading	Effective Depth, L (cm)
1.000	16.3
1.001	16.0
1.002	15.8
1.003	15.5
1.004	15.2
1.005	12.0
1.006	14.7
1.007	14.4
1.008	14.2
1.009	13.9
1.010	13.7
1.011	13.4
1.012	13.1
1.013	12.9
1.014	12.6
1.015	12.3
1.016	12.1
1.017	11.8
1.018	11.5
1.019	11.3
1.020	11.0
1.021	10.7
1.022	10.5
1.023	10.2
1.024	10.0
1.025	9.7
1.026	9.4
1.027	9.2
1.028	8.9
1.029	8.6
1.030	8.4
1.031	8.1
1.032	7.8
1.033	7.6
1.034	7.3
1.035	7.0

APPENDIX B: SPECTRAL ANALYSIS

B.1 Using Gamma Vision Software to Determine Sample Radionuclide Activities

The activity of each sample was determined through the use of Gamma Vision Software. This software package allows the user to analyze a spectrum of radionuclide activities that a sample contains. The program breaks each activity into a series of channels (represented by a single vertical bar) that correspond to a unique wavelength energy of a particular radionuclide (Figure B.1 and Figure B.2). Within this spectrum, the peak activities of the radionuclide of interest, in this case ^{137}Cs and ^{210}Pb, can be identified, and the area of the each peak can be calculated within the GammaVision Package. The procedures to complete this are as follows:

1. Open GammaVision Buffer
2. File
    a. Recall
    b. Open Sample File Recorded by Gamma Detector
3. Once the Sample Spectrum (See Figure B.1) is Open
    a. Identify the Peak in question (Figure B.2)
    b. Isolate Peak (±11 Channels from peak for ^{137}Cs and ±9 for ^{210}Pb)
4. Once Peak is Highlighted
    a. Click Info
    b. Record Values (Figure B.3)
        1. Net Area
        2. Error

Once these values are obtained they can be used in determining the activity of each sample as outlined in Chapter 3 of this thesis.

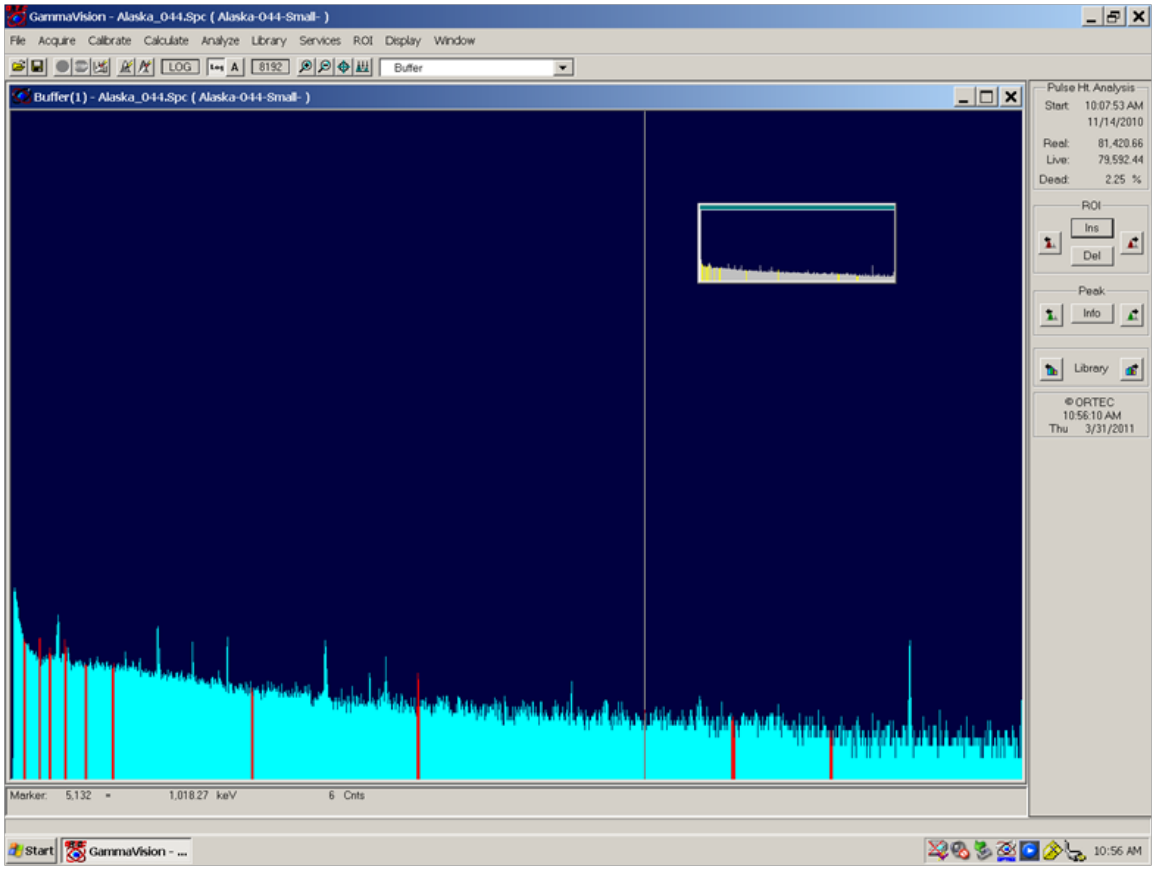

Figure B.1: Screen Shot of Gamma Vision Spectrum for Sample 44

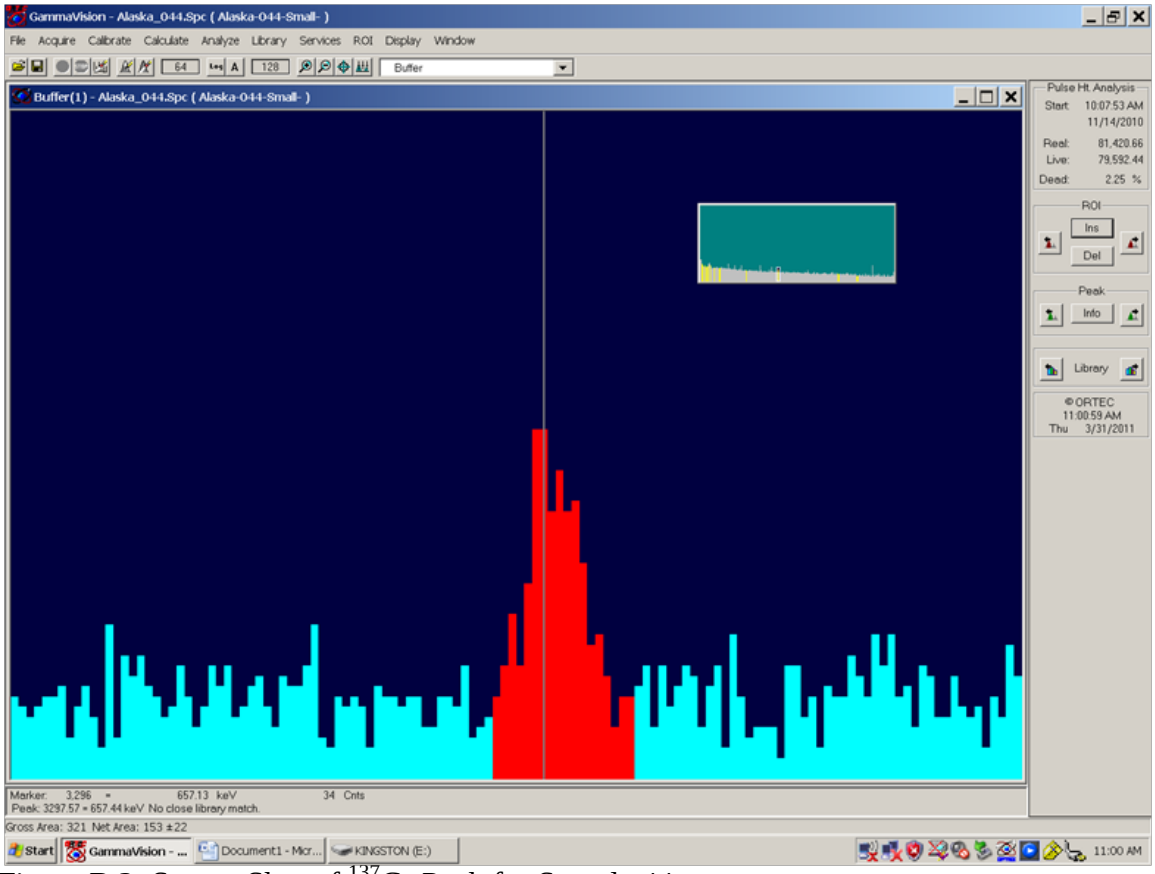

Figure B.2: Screen Shot of ^{137}Cs Peak for Sample 44

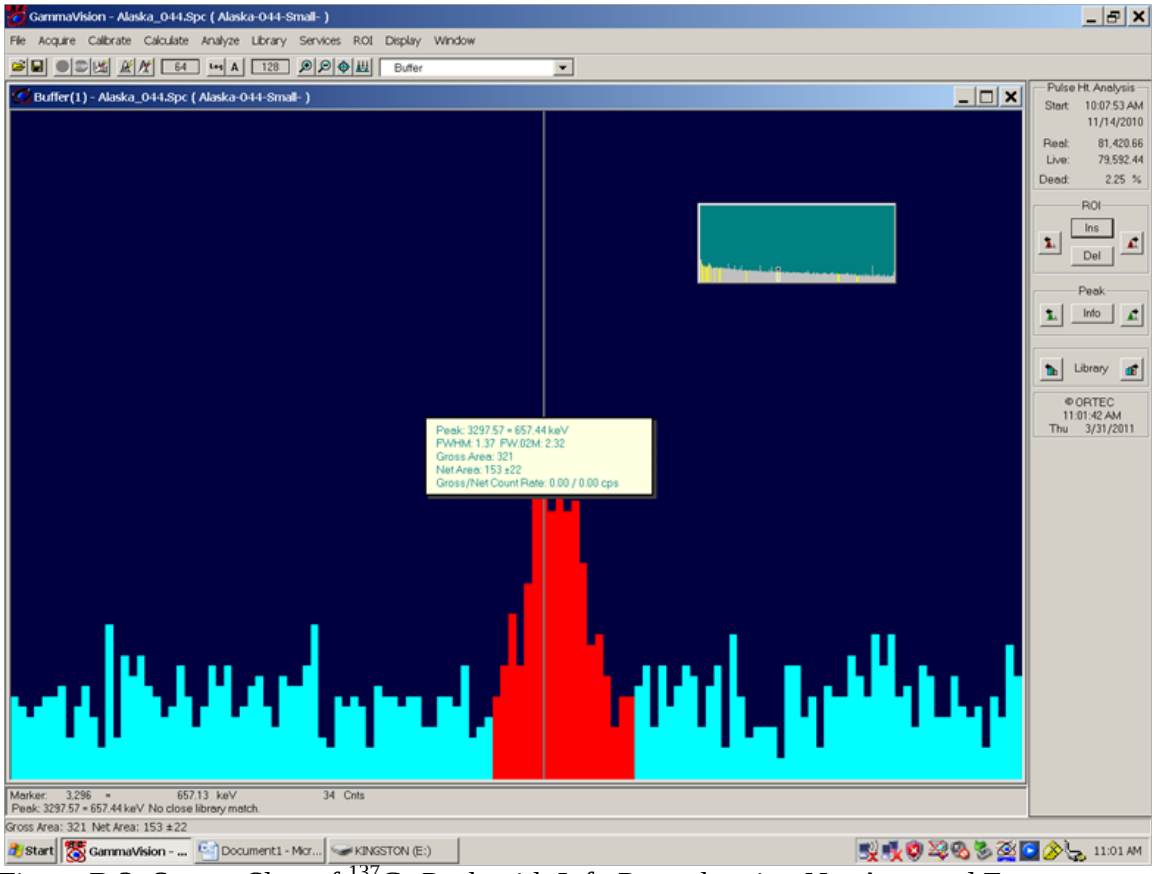

Figure B.3: Screen Shot of ^{137}Cs Peak with Info Pane showing Net Area and Error Readings

APPENDIX C: POROSITY AND BULK DENSITY OF SAMPLES

C.1 Calculation of Porosity and Bulk Density

As described in Chapter 3 of this thesis, sample cores were collected from Black Lake, AK to analyze sedimentation rates within the catchment. In addition to determining these rates, it is also important to understand the characteristics of the soil being deposited there. Two such characteristics are the porosity (P) and bulk density. The method for finding Porosity is described by Eq. 3.1. The Equation for Bulk density is as follows:

$$\rho_{BD} = \frac{M_s}{V_t} \qquad \text{Eq C.1}$$

where ρ_{BD} is the bulk density, M_s is the sample mass, and V_t is the sample volume. These values further help in determining how compact the incoming sediment is and how what types of soils they are based on the density. Typical values for the bulk density of quartz and mineral type soils (e.g. clays) are roughly 2.65 (g/cm^3) and 1.0 to 1.6 (g/cm^3), respectively (Chang, 2002). Table C.1 below lists all of the samples tested for radionuclide activity along with their respective porosity and bulk density:

Table C.1: Activity, Weight, Porosity, and Bulk Density Results for Crooked Creek

Sample #	Site	Upper Depth	Lower Depth	Wet Weight	Dry Weight	Excess Activity (Bq/g)	Cs-137 Activity (Bq/g)	Porosity	Bulk Density
1	Crooked Creek	0	2.5	102.598	53.016	0.005	0.005	98%	1.05
2	Crooked Creek	2.5	5	88.024	41.865	0.009	0.003	91%	0.83
3	Crooked Creek	5	7.5	92.258	45.592	0.010	0.006	92%	0.90
4	Crooked Creek	7.5	10	108.8	52.885	0.011	0.008	110%	1.04
5	Crooked Creek	10	12.5	115.096	65.044	0.012	0.004	99%	1.28
6	Crooked Creek	12.5	15	112.74	70.150	0.004	0.005	84%	1.38

Table C.2: Activity, Weight, Porosity, and Bulk Density Results for Cottonwood Creek

Sample #	Site	Upper Depth	Lower Depth	Wet Weight	Dry Weight	Excess Activity (Bq/g)	Cs-137 Activity (Bq/g)	Porosity	Bulk Density
17	Cottonwood	22.5	25	97.64	52.364	0.003	0.007	89%	1.03
19	Cottonwood	27.5	30	126.603	81.690	0.000	0.003	89%	1.61

Table C.3: Activity, Weight, Porosity, and Bulk Density Results for Linhome Creek

Sample #	Site	Upper Depth	Lower Depth	Wet Weight	Dry Weight	Excess Activity (Bq/g)	Cs-137 Activity (Bq/g)	Porosity	Bulk Density
39	Linhome	30	32.5	140.944	92.094	0.008	0.000	96%	1.82

Table C.4: Activity, Weight, Porosity, and Bulk Density Results for A2

Sample #	Site	Upper Depth	Lower Depth	Wet Weight	Dry Weight	Excess Activity (Bq/g)	Cs-137 Activity (Bq/g)	Porosity	Bulk Density
41	A2	2.5	5	104.346	80.797	0.004	0.003	46%	1.59
43	A2	7.5	10	127.148	91.377	0.016	0.004	71%	1.80
44	A2	10	12.5	118.721	86.479	0.017	0.004	64%	1.71
45	A2	12.5	15	115.042	80.791	0.007	0.003	68%	1.59

Table C.5: Activity, Weight, Porosity, and Bulk Density Results for Canoe Creek

Sample #	Site	Upper Depth	Lower Depth	Wet Weight	Dry Weight	Excess Activity (Bq/g)	Cs-137 Activity (Bq/g)	Porosity	Bulk Density
79	Canoe	0	2.5	72.572	31.349	0.072	0.013	81%	0.62
80	Canoe	2.5	5	69.206	27.025	0.086	0.054	83%	0.53
81	Canoe	5	7.5	91.569	42.227	0.025	0.024	97%	0.83
82	Canoe	7.5	10	101.576	51.223	0.020	0.005	99%	1.01
83	Canoe	10	12.5	97.461	53.323	0.013	0.003	87%	1.05
84	Canoe	12.5	15	90.664	46.698	0.013	0.002	87%	0.92
85	Canoe	15	17.5	113.741	70.014	0.012	0.001	86%	1.38
86	Canoe	17.5	20	121.38	82.347	0.000	0.000	77%	1.63
87	Canoe	20	22.5	122.364	82.510	0.001	0.000	79%	1.63
88	Canoe	22.5	25	115.62	75.180	0.005	0.000	80%	1.48
89	Canoe	25	27.5	123.134	74.478	0.000	0.000	96%	1.47
91	Canoe	30	32.5	113.538	75.629	0.006	0.000	75%	1.49

Table C.6: Activity, Weight, Porosity, and Bulk Density Results for A4

Sample #	Site	Upper Depth	Lower Depth	Wet Weight	Dry Weight	Excess Activity (Bq/g)	Cs-137 Activity (Bq/g)	Porosity	Bulk Density
93	A4	0	2.5	82.096	67.188	0.002	0.001	29%	1.33
94	A4	2.5	5	90.643	73.912	0.017	0.001	33%	1.46
95	A4	5	7.5	86.181	59.422	0.021	0.002	53%	1.17
96	A4	7.5	10	106.173	73.267	0.027	0.003	65%	1.45
97	A4	10	12.5	96.529	70.938	0.008	0.002	51%	1.40
98	A4	12.5	15	95.127	68.626	0.024	0.001	52%	1.35
99	A4	15	17.5	103.132	69.616	0.020	0.003	66%	1.37
100	A4	17.5	20	108.872	77.410	0.002	0.003	62%	1.53
101	A4	20	22.5	104.635	72.305	0.013	0.004	64%	1.43
102	A4	22.5	25	101.849	66.745	0.021	0.003	69%	1.32
103	A4	25	27.5	97.15	60.237	0.006	0.003	73%	1.19
104	A4	27.5	30	119.58	82.443	0.014	0.004	73%	1.63
105	A4	30	32.5	100.501	65.852	0.010	0.003	68%	1.30
106	A4	32.5	35	100.847	59.832	0.008	0.000	81%	1.18
107	A4	35	37.5	110.702	69.615	0.004	0.000	81%	1.37
108	A4	37.5	40	104.648	67.694	0.001	0.000	73%	1.34
109	A4	40	42.5	119.097	76.407	0.002	0.000	84%	1.51
110	A4	42.5	45	142.952	94.770	0.000	0.000	95%	1.87

Table C.7: Activity, Weight, Porosity, and Bulk Density Results for NFD Up

Sample #	Site	Upper Depth	Lower Depth	Wet Weight	Dry Weight	Excess Activity (Bq/g)	Cs-137 Activity (Bq/g)	Porosity	Bulk Density
111	NFD Up	0	2.5	96.404	57.582	0.048	0.005	77%	1.14
112	NFD Up	2.5	5	83.117	43.386	0.047	0.004	78%	0.86
113	NFD Up	5	7.5	95.215	55.588	0.052	0.005	78%	1.10
114	NFD Up	7.5	10	99.254	61.753	0.037	0.004	74%	1.22
115	NFD Up	10	12.5	113.519	86.979	0.014	0.002	52%	1.72
116	NFD Up	12.5	15	118.022	91.046	0.010	0.001	53%	1.80

Table C.8: Activity, Weight, Porosity, and Bulk Density Results for SFD Up

Sample #	Site	Upper Depth	Lower Depth	Wet Weight	Dry Weight	Excess Activity (Bq/g)	Cs-137 Activity (Bq/g)	Porosity	Bulk Density
130	SFD Up	0	2.5	31.338	13.809	0.068	0.005	35%	0.27
131	SFD Up	2.5	5	59.608	26.435	0.231	0.018	65%	0.52
132	SFD Up	5	7.5	73.625	37.505	0.095	0.029	71%	0.74
133	SFD Up	7.5	10	77.375	40.290	0.025	0.012	73%	0.80
134	SFD Up	10	12.5	108.093	66.586	0.004	0.002	82%	1.31
135	SFD Up	12.5	15	103.607	59.509	0.013	0.000	87%	1.17
136	SFD Up	15	17.5	94.218	69.254	0.010	0.000	49%	1.37
138	SFD Up	20	22.5	106.255	64.112	0.000	0.000	83%	1.27
139	SFD Up	22.5	25	102.821	57.047	0.002	0.001	90%	1.13
140	SFD Up	25	27.5	112.895	64.489	0.000	0.000	96%	1.27
141	SFD Up	27.5	30	103.873	57.171	0.000	0.000	92%	1.13
142	SFD Up	30	32.5	114.871	67.440	0.015	0.001	94%	1.33
143	SFD Up	32.5	35	123.388	82.613	0.002	0.000	80%	1.63
144	SFD Up	35	37.5	108.1	63.817	0.011	0.000	87%	1.26
145	SFD Up	37.5	40	108.493	60.610	0.005	0.001	94%	1.20
146	SFD Up	40	42.5	108.34	65.063	0.000	0.000	85%	1.28
147	SFD Up	42.5	45	56.972	36.990	0.009	0.000	39%	0.73

Table C.9: Activity, Weight, Porosity, and Bulk Density Results for Outlet

Sample #	Site	Upper Depth	Lower Depth	Wet Weight	Dry Weight	Excess Activity (Bq/g)	Cs-137 Activity (Bq/g)	Porosity	Bulk Density
148	Outlet	0	2.5	125.676	91.212	0.010	0.001	68%	1.80
149	Outlet	2.5	5	128.493	86.009	0.005	0.000	84%	1.70
150	Outlet	5	7.5	147.614	113.560	0.000	0.000	67%	2.24
151	Outlet	7.5	10	141.312	111.790	0.000	0.000	58%	2.21
152	Outlet	10	12.5	141.995	111.646	0.001	0.000	60%	2.20
153	Outlet	12.5	15	137.567	106.470	0.006	0.000	61%	2.10
154	Outlet	15	17.5	136.992	107.175	0.009	0.000	59%	2.12
155	Outlet	17.5	20	118.098	88.962	0.001	0.000	58%	1.76
156	Outlet	20	22.5	135.023	105.283	0.000	0.001	59%	2.08
157	Outlet	22.5	25	133.625	105.463	0.004	0.000	56%	2.08
158	Outlet	25	27.5	137.507	102.335	0.000	0.000	69%	2.02
159	Outlet	27.5	30	135.236	100.360	0.000	0.000	69%	1.98
161	Outlet	32.5	35	127.291	95.690	0.000	0.000	62%	1.89
162	Outlet	35	37.5	132.817	98.778	0.000	0.000	67%	1.95

Table C.10: Activity, Weight, Porosity, and Bulk Density Results for NFD Old

Sample #	Site	Upper Depth	Lower Depth	Wet Weight	Dry Weight	Excess Activity (Bq/g)	Cs-137 Activity (Bq/g)	Porosity	Bulk Density
165	NF Old	0	2.5	103.08	63.820	0.021	0.003	77%	1.26
166	NF Old	2.5	5	114.307	80.250	0.012	0.002	67%	1.58
168	NF Old	7.5	10	110.737	83.714	0.011	0.000	53%	1.65
169	NF Old	10	12.5	119.044	90.483	0.008	0.000	56%	1.79
170	NF Old	12.5	15	124.917	95.354	0.003	0.000	58%	1.88
171	NF Old	15	17.5	119.245	87.114	0.009	0.000	63%	1.72
172	NF Old	17.5	20	121.237	83.526	0.000	0.000	74%	1.65
173	NF Old	20	22.5	122.897	86.519	0.007	0.002	72%	1.71
174	NF Old	22.5	25	113.836	85.794	0.009	0.002	55%	1.69
175	NF Old	25	27.5	119.889	81.690	0.007	0.001	75%	1.61
176	NF Old	27.5	30	122.784	84.211	0.016	0.000	76%	1.66
177	NF Old	30	32.5	126.798	94.132	0.009	0.000	64%	1.86
178	NF Old	32.5	35	122.076	87.696	0.000	0.000	68%	1.73
179	NF Old	35	37.5	110.390	81.150	0.006	0.001	58%	1.60
181	NF Old	40	42.5	97.519	56.082	0.010	0.003	82%	1.11

Table C.11: Activity, Weight, Porosity, and Bulk Density Results for SF Down

Sample #	Site	Upper Depth	Lower Depth	Wet Weight	Dry Weight	Excess Activity (Bq/g)	Cs-137 Activity (Bq/g)	Porosity	Bulk Density
184	SF Down	0	2.5	95.665	65.219	0.019	0.003	60%	1.29
185	SF Down	2.5	5	115.600	77.077	0.014	0.000	76%	1.52
186	SF Down	5	7.5	112.788	84.375	0.003	0.000	56%	1.67
187	SF Down	7.5	10	104.800	74.087	0.015	0.001	61%	1.46
191	SF Down	17.5	20	107.929	78.040	0.016	0.001	59%	1.54
192	SF Down	20	22.5	113.481	84.877	0.004	0.001	56%	1.68
195	SF Down	27.5	30	114.753	85.795	0.007	0.002	57%	1.69
197	SF Down	32.5	35	114.472	85.916	-0.002	0.002	56%	1.70
199	SF Down	37.5	40	120.792	90.194	0.003	0.001	60%	1.78

Table C.12: Activity, Weight, Porosity, and Bulk Density Results for NF New

Sample #	Site	Upper Depth	Lower Depth	Wet Weight	Dry Weight	Excess Activity (Bq/g)	Cs-137 Activity (Bq/g)	Porosity	Bulk Density
202	NF New	2.5	5	110.789	83.573	0.006	0.001	54%	1.65
203	NF New	5	7.5	106.570	86.338	0.009	0.000	40%	1.70
207	NF New	15	17.5	109.972	82.174	0.007	0.002	55%	1.62
210	NF New	22.5	25	110.680	87.118	0.000	0.001	46%	1.72
216	NF New	37.5	40	114.553	83.848	0.005	0.000	61%	1.65

BIBLIOGRAPHY

Agapkina, G.I., Tikhomirov, F.A., Shcheglov, A.I., Kracke, W., & Bunzl, K. (1995). Association of chernobyl-derived pu-239+240, am-241, sr-90 and cs-137 with organic matter in the soil solution. *Journal of Environmental Radioactivity*, *29*, 257-269.

Balistrieri, L.S., & Murray, J.W. (1984). Marine scavenging: trace metal adsorption by interfacial sediment from manop site h1. *Geochimica et Cosmochimica Acta*, *48*, 921-929.

Begy, R, Cosma, C, & Timar, A. (2009). Recent changes in red lake (Romania) sedimentation rate determined from depth profiles of 210pb and 137cs radioisotopes. *Journal of Environmental Radioactivity*, *100*(8), 644-648.

Behrens, E.W. (1980). On sedimentation rates and porosity. *Geology*., 35, Mll--M16.

Bonniwell, E.C., Matisoff, G., & Whiting, P.J. (1999). Determining the times and distances of particle transit in a mountain stream using fallout radionuclides. *Geomorphology*, *27*(1-2), 75-92.

Buffington, J.M. (2002). *Geomorphic reconnaissance of the black lake area, alaska peninsula*. Boise, ID: The University of Idaho.

Chang, H.H. (2002). *Fluvial processes in river engineering*. Krieger Publishing Company.

Chignik Topo Maps A5 and B4. (2011). Retrieved from http://www.trails.com/topo.aspx?lat=56.21083&lon=-159.48917&s=100&size=s

Cutshall, N.H., Larsen, I.L., & Olsen, C.R. (1983). Direct analysis of pb-210 in sediment samples - self-adsorption corrections. *Nuclear Instruments and Methods in Physics Research*, *206*(1-2), 309-312.

Denn, K.D. (2010). *Sediment budget closure during runoff-generated high flow events in the south amana sub-watershed, ia*. Iowa City, IA: University of Iowa.

Edmondson, W.T., Anderson, G.C., & Peterson, D.R. (1956). Artificial eutrophication of lake washington. *Limnology and Oceanography*, *1*, 47-53.

Elhakeem, M., & Papanicolaou, A.N. (2008). Evaluation of the reduction in the water storage capacity of black lake, AK. International Journal of River Basin Management, 6(1), 63-77.

Fauer, G. (1986). *Principles of isotope geochemistry*. New York, NY: John Wiley and Sons.

Golosov, V.N., Walling, D.E., Panin, A.V., Stukin, E.D., & Kvasnikova, E.V., Ivanova, N.N. (1999). The spatial variability of chernobyl derived cs137 inventories in a small agricultural drainage basin in central russia. *Applied Radiation and isotopes*, *51*(3), 341-352.

Google Earth Pro. 2011. Alaska Depicting Black Lake. Google, Inc. Mountain View California.

Google Earth Pro. 2011. Black Lake Depicting Tributaries. Google, Inc. Mountain View California.

Google Earth Pro. 2011. Black lake Depicting Sample Sites and Sedimentation Rates. Google, Inc. Mountain View California.

Griffiths, J.R., Schindler, D.E., Balistieri, L.S., & Ruggerone, G.T. (2011). Effects of simultaneous climate change and geomorphic evolution in thermal characteristics of a shallow alaskan lake. *Limnology and Oceanography*, *56*(1), 193-205.

He, Q., & Walling, D.E. (1996). Interpreting particle size effects in the adsorption of cs-137 and unsupported pb-210 by mineral soils and sediments. *Journal of Environmental Radioactivity*, *30*, 117-137.

Hooke, R.L. (1994). On the efficacy of humans as geomorphic agents. *GSA Today*, *4*(9), 218-225.

Horne, A.J., & Goldman, C.R. (1994). *Limnology*. New York, NY: McGraw-Hill, Inc.

Huang, C., Wells, L.K., & Norton, L.D. (1999). Sediment transport capacity and erosion processes: model concepts and reality. *Earth Surface Processes and landforms*, *24*, 503-516.

Hughes, A.O., Olley, J.M., Croke, J.C., & Wenster, I.T. (2009). Determining floodplain sedimentation rates using 137cs in a low fallout environment dominated by channel- and cultivation-derived sediment inputs, central Queensland, Australia. *Journal of Environmental Radioactivity*, *100*(10), 858-865.

Jin, K.R., & Sun, D. (2007). Sediment resuspension and hydrodynamics in lake okeechobee during late summer. *journal of engineering mechanics*, *133*(8), 899-910.

Julien, R.Y., & Simons, D.B. (1985). Sediment transport capacity of overland flows. *Transactions of the ASCE, 28*, 755-762.

Kanai, Y. (2011). Characterization of 210pb and 137cs radionuclides in sediment from lake shinji, shimane prefecture, western japan . Applied Radiation and Isotopes, 69(2), 455-462.

Kendall, C., & McDonnell, J. (1998). *Isotope tracers in catchment hydrology*. New York, NY: Elsevier.

Ketterer, M.E., Hafer, K.M., Link, C.L., Royden, C.S., & Hartsock, W.J. (2003). Anthropogenic 236u at rocky flats, ashtabula river harbor, and mersey estuary: three case studies by sector inductively coupled plasma mass spectrometry. *Journal of Environmental Radioactivity*, *67*(3), 191-206.

Kuhnle, R.A., Bingner, R.L., Alonso, C.V., Wilson, C.G., & Simon, A. (2008). Conservation practice effects on sediment load in the goodwin creek experimental watershed. Journal of Soil and Water Conservation, 63(6), 496-503.

Lal, R. (2005). Soil erosion and carbon dynamics. *Soil & Tillage Research*, *81*, 137-142.

Li, S., Lobb, D.A., Kachanoski, R.G., & McConkey, B.G. (2011). Comparing the use of the traditional and repeated-sampling-approach of the 137cs technique in soil erosion estimation. Geoderma, 160(3-4), 324-335.

Mabit, L., Benmansour, M., & Walling, D.E. (2008). Comparative advantages and limitations of the fallout radionuclides 137cs, 210pbex and 7be for assessing soil erosion and sedimentation. Journal of Environmental Radioactivity, 99(12), 1799-1807.

Meade, R.H., Day, T.J., Riggs, H.C., & Yuzyk, T.R. (1990). Movement and storage of sediment in rivers of the united states and canada. *Proceedings of the Geological society of america* (pp. 255-280). Boulder, CO: M.G. Wolman.

Mizugaki, S., Nakamura, F., & Araya, T. (2006). Using dendrogeomorphology and 137cs and 210pb radiochronology to estimate recent changes in sedimentation rates in kushiro mire, northern japan, resulting from land use change and river channelization . Catena, 68(1), 25-40.

Porto, P., Walling, D.E., & Ferro, V. (2001). Validating the use of caesium-137 measurements to estimate soil erosion rates in a small drainage basin in calabria, southern italy. Journal of Hydrology, 248(1-4), 93-108.

Rabalais, N.N., Diaz, R.J., Levin, L.A., Turner, R.E., Gilbert, D., & Zhang, J. (2010). Dynamics and distribution of natural and human-caused coastal hypoxia. *Biogeosciences, 19*, 215-233.

Richie, J.C., & McHenry, J.R. (1990). Application of radioactive fallout cesium-137 for measuring soil erosion and sediment accumulation rates and patterns: a review. *Journal of Environmental Quality, 19*, 585-619.

Robbins, J.A., McCall, P.L., Fisher, J.B., & Krezoski, J.R. (1979). Effect of deposit feeders on migration of 137cs in lake sediments. *Earth and Planetary Science, 42*, 277-287.

Ruggerone , G.T. (1994). Investigations of salmon populations, hydrology, and limnology of the chignik lake, alaska, during 1993. *Proceedings of the Chignik regional aquaculture association* Natural Resources Consultants, Inc.

Ruggerone , G.T. (2003). Rapid natural habitat degradation and consequences for sockeye salmon production in the chignik lakes system, alaska. *Proceedings of the Chignik regional aquaculture association*

Ruggerone, J.C., Steen, R., & Hilborn, R. National Marine Fisheries Service, (1999). *Chignik salmon studies investigations of salmon populations, hydrology, and limnology of the chignik lakes, alaska*. Juneau, AK:

Sanders, C.J., Santos, I.R., Sambasiva, R., Schaefer, C., & Silva-Filho, E.V. (2010). Recent 137cs deposition in sediments of admiralty bay, Antarctica. *Journal of Environmental Radioactivity, 101*(5), 87-103.

Santschi, P.H., Bollhalder, S., Zingg, S., Luck, A., & Farrenkothen, K. (1989). The self-cleaning capacity of surface waters after radioactive fallout. evidence from european waters after chernobyl, 1986-1988. *Environmental Science and Technology*, *24*(4), 519-527.

Shukla, B.S. (1996). *Sedimentation rate through environmental radioactivity: 210pb dating of sediments.* Hamilton, ON, Canada: Environmental Research & Publication Inc.

Stallard, R.F. (1998). Terrestrial sedimentation and the carbon cycle: coupling weathering and erosion to carbon burial. *Global Biogeochemical Cycles*, *12*(2), 231-257.

Stihler, S.D., Stone, D.B., & Beget, J.E. (1992). Varve counting vs tephrochronology and cs-137 and pb-210 dating - a comparative test at skilak lake, alaska. *Geology*, *20*, 1019-1022.

Sugai, S.F. (1990). Transport and sediment accumulation of 210pb and 137cs in two southeast alaskan fjords. *Estuaries*, *13*, 380-392.

Taylor, J.R. (1997). *An introduction to error analysis: the study of uncertainties in physical measurements*. Sausalito, CA: University Science Books.

Todd, J.F., Wong, G.T.F., Olsen, C.R., & Larsen, I.L. (1989). Atmospheric depositional characteristics of beryllium-7 and lead-210 along the southeastern virginia coast. *Journal of Geophysical Research*, *94*(D8), 11106-11116.

Veniaminof description and statistics. (2011). Retrieved from http://www.avo.alaska.edu/volcanoes/volcinfo.php?volcname=Veniaminof

Wallbrink, P.J., & Murray, A.S. (1993). Use of fallout radionuclides as indicators of erosion processes. *Hydrological Processes*, *7*(3), 297-304.

Walling, D.E., Collings, A.L., & Sichingabula, H.M. (2003). Using unsupported lead-210 measurements to investigate soil erosion and sediment delivery in a small zambian catchment . Geomorphology, 104(3-4), 262-275.

Wilson, C.G., Matisoff, G., & Whiting, P.J. (2003). Short-term erosion rates from a be-7 inventory balance. *Earth Surface Processes and Landforms*, *28*(9), 967-977.

Wilson, C.G., Matisoff, G., & Whiting, P.J. (2005). The 7be/210pbxs ratio as an indicator of suspended sediment age or fraction new sediment in suspension. *Earth Surface Processes and Landforms*, *30*(9), 1191-1201.